doi:10.1093/brain/awaa404 BRAIN 2021: 144; 615–635 | 615

BRAIN
A JOURNAL OF NEUROLOGY

Stepwise crosstalk between aberrant Nf1, Tp53 and Rb signalling pathways induces gliomagenesis in zebrafish

Juanjuan Luo,[1,2,†] Pei Liu,[1,†] Chunjiao Lu,[1] Wanping Bian,[2] Dongsheng Su,[1,2] Chenchen Zhu,[1] Shaolin Xie,[2] Yihang Pan,[3] Ningning Li,[3] Wei Cui,[4] De-Sheng Pei[2] and Xiaojun Yang[1]

[†]These authors contributed equally to this work.

The molecular pathogenesis of glioblastoma indicates that RTK/Ras/PI3K, RB and TP53 pathways are critical for human gliomagenesis. Here, several transgenic zebrafish lines with single or multiple deletions of *nf1*, *tp53* and *rb1* in astrocytes, were established to genetically induce gliomagenesis in zebrafish. In the mutant with a single deletion, we found only the *nf1* mutation low-efficiently induced tumour incidence, suggesting that the Nf1 pathway is critical for the initiation of gliomagenesis in zebrafish. Combination of mutations, *nf1*;*tp53* and *rb1*;*tp53* combined knockout fish, showed much higher tumour incidences, high-grade histology, increased invasiveness, and shortened survival time. Further bioinformatics analyses demonstrated the alterations in RTK/Ras/PI3K, cell cycle, and focal adhesion pathways, induced by abrogated *nf1*, *tp53*, or *rb1*, were probably the critical stepwise biological events for the initiation and development of gliomagenesis in zebrafish. Gene expression profiling and histological analyses showed the tumours derived from zebrafish have significant similarities to the subgroups of human gliomas. Furthermore, temozolomide treatment effectively suppressed gliomagenesis in these glioma zebrafish models, and the histological responses in temozolomide-treated zebrafish were similar to those observed in clinically treated glioma patients. Thus, our findings will offer a potential tool for genetically investigating gliomagenesis and screening potential targeted anti-tumour compounds for glioma treatment.

1 Neuroscience Center, Shantou University Medical College, Shantou 515041, China
2 Chongqing Institute of Green and Intelligent Technology, Chinese Academy of Sciences, Chongqing 400714, China
3 The Seventh Affiliated Hospital of Sun Yat-sen University, Shenzhen 518107, China
4 Department of Pharmacology, College of Life Science and Biopharmaceutical of Shenyang Pharmaceutical University, Shenyang 110016, China

Correspondence to: Xiaojun Yang, PhD
Neuroscience Center, Shantou University Medical College
Shantou 515041, China
E-mail: yangx@stu.edu.cn

Correspondence may also be addressed to: De-Sheng Pei, PhD
Chongqing Institute of Green and Intelligent Technology, Chinese Academy of Sciences
Chongqing 400714, China
E-mail: peids@cigit.ac.cn

Keywords: nf1; rb1; tp53; glioma; zebrafish

Abbreviations: (c)KO = (combined) knockout; dpf = days post-fertilization; TMZ = temozolomide

Received May 17, 2020. Revised August 19, 2020. Accepted September 15, 2020. Advance access publication December 5, 2020

Introduction

Malignant gliomas are the most frequently occurring brain tumours in the CNS, with both high recurrence and mortality rates (Ostrom *et al.*, 2018). According to the WHO criteria, gliomas can be histologically classified as grade I to IV (Diamandis and Aldape, 2018). Grade IV diffuse gliomas, which are also known as primary glioblastoma, are due to the development of pre-existing low-grade gliomas (Ohgaki and Kleihues, 2013), and associated with <10% long-term survival (Thurnher, 2009).

Tumorigenesis is known to be induced by the sequential accumulation of genetic alterations, including functional dysregulation of tumour suppressors, and activation of growth factor or survival signalling pathways (Gladson *et al.*, 2010). The molecular pathogenesis of glioblastoma indicates that the dysregulation of three core pathways, including receptor tyrosine kinase (RTK)/Ras/phosphatidylinositol 3′-kinase (PI3K), RB, and TP53 pathway, are critically detected in most glioblastoma patients (Cancer Genome Atlas Research, 2008; Parsons *et al.*, 2008). Among these pathways, the RTK/Ras/PI3K pathway is associated with many tumour-related key kinase intermediates, such as EGFR amplification and PTEN loss (Brisbin *et al.*, 2009; Ye *et al.*, 2016). Additionally, as a PI3K downstream target, AKT has more than 40 tumour-related downstream targets, including FOXO, GSK-3β, mTOR, and TSC1/2 (Manning and Cantley, 2007). The mutation of NF1, a key regulator of the RTK/Ras/PI3K pathway, can lead to the increasing mesenchymal phenotype, and enhanced motility and invasion in various malignant tumours (Symons and Segall, 2009; Yamazaki *et al.*, 2009). *RB1* gene mutations were also detected in many human malignant tumours, especially at the early stage. Phosphorylated RB1 restrains proliferation by repressing E2F transcription factors, and regulates many biological processes, including metabolism and apoptosis by interacting with several transcription factors (Dyson, 2016). Aberrant RB1 expression can result in decreased tangential migration of neurons, enhanced invasiveness in prostate cancer, and increased aggressiveness in ovarian cancer (Ferguson *et al.*, 2005; Comisso *et al.*, 2017; Thangavel *et al.*, 2017). It is well known that the aberration of TP53 expression or activity is associated with tumorigenesis in most malignant tumours (Vousden and Lu, 2002; Muller and Vousden, 2013). A previous study showed that the alterations of the RB and TP53 pathways are associated with high proliferation in bladder urothelial carcinoma (Goussia *et al.*, 2018). The inhibition of TP53 and/or AKT can result in the rapid death of alternative lengthening of telomeres (ALT)-related cancer cells (Ge *et al.*, 2019).

Several studies have illustrated the effects of *Nf1*, *Rb1*, or *Tp53* deletion in animal models. Telencephalon-specific *Rb1* knockout (KO) results in enhanced neurogenesis and abnormal cortical development (Ferguson *et al.*, 2002). MacPherson *et al.* (2003) found the conditional mutation of *Rb1* leads to cell cycle defects, which are primarily characterized by increased proliferation in CNS of mouse embryos. Solin *et al.* (2015) generated glial-like tumours by gene editing nuclease somatic targeting of the tumour suppressor *rb1* in zebrafish, and Schultz *et al.* (2018) further demonstrated that somatic editing is a viable approach to induce tumorigenesis in zebrafish. In addition, the mutation of *Nf1* alone results in lower-grade glioma, suggesting that the aberrant NF1 signalling is likely associated with gliomagenesis (D'Angelo *et al.*, 2019). A previous study also showed that the ablation of *Nf1* was positively linked to the tumorigenesis of malignant peripheral nerve sheath tumours (Shin *et al.*, 2012). In a murine model with the *Tp53* deletion mutation, the pleiotropic accumulation of cooperative oncogenic alterations induced gliomagenesis (Wang *et al.*, 2009). Moreover, malignant gliomas were found to be induced by the conditional deletion of *Tp53* combined with haploinsufficiency of *Pten* and *Nf1* in transgenic mice (Alcantara Llaguno *et al.*, 2009). Chow *et al.* (2011) induced various combinations of *Tp53*, *Pten* or *Rb1* mutations in astrocytes and neural precursors in mature mice, which ultimately resulted in high-grade gliomas.

Over recent decades, zebrafish have become an increasingly popular animal model of various diseases, including leukaemia, hepatocellular carcinoma, melanoma, and Alzheimer's disease (Langenau *et al.*, 2003; Patton *et al.*, 2005; Bai *et al.*, 2007; Paquet *et al.*, 2009; Li *et al.*, 2012*b*). In this context, the glioma transgenic zebrafish model was first established using a transgenic approach involving the activation of Akt1 alone in zebrafish (Jung *et al.*, 2013). However, several limitations, including the lack of genetic definition, the lower efficiency of tumour incidence, and the single oncogenic factor, attenuate its utility for studying gliomagenesis with various mutational spectra. Here, we used the CRISPR/Cas9 strategy to establish several transgenic zebrafish lines with glial fibrillary acidic protein (*gfap*) promoter-driving tissue-specific *nf1*, *rb1*, or *tp53* mutation, and further precisely investigated gliomagenesis in the mature brain with deficiencies in Nf1a, Tp53, and/or Rb1 in zebrafish. Our results demonstrated that various combinations of *nf1*, *tp53* and/or *rb1* mutations can induce grade I to IV gliomas with different typical phenotypes. Further gene expression profiling defined the molecular features of the gliomas derived from zebrafish, which has significant similarity to the corresponding subgroups in human gliomas. Thus, these genetically defined zebrafish models might be helpful for studying the gliomagenesis with various mutational spectra.

Materials and methods

Strains, husbandry, breeding and drug treatment

The wild-type zebrafish line (AB strain) and *Tg*(*gfap*:*GFP*) transgenic fish (Bernardos and Raymond, 2006) were obtained from the China Zebrafish Resource Center (Wuhan, China), and raised according to the guidelines for zebrafish care

(Westerfield, 2007). Fish were maintained in a large-scale water-recirculating system under a 14-h light/10-h dark cycle at 28°C. The juvenile and adult fish (>15 days post-fertilization; dpf) were kept in system water (40 g sea salts/l in deionized water, pH 7.0, salinity 0.03%, and conductivity 500 μS) in serial tanks at densities of five fish per litre (60 fish/12 l). The fish were fed two to three times daily with a rich supply of freshly hatched brine shrimp. For zebrafish breeding, the healthy fish (three males and three females) at 3–4 months of age were selected to produce embryos in each breeding tank on the day before breeding. Following the start of the next light cycle, the embryos were collected by siphoning the bottom of the tank. The embryos (⩽4 dpf) and larvae (5–15 dpf) were maintained in E3 embryonic medium (5 mM NaCl, 0.17 mM KCl, 0.33 mM $CaCl_2$ and 0.33 mM $MgSO_4$ in deionized water) with 10^{-5}% methylene blue in 90-mm Petri dishes (50 embryos or 10 larvae per dish) at 28°C, and fed with paramecia (4–9 dpf) and brine shrimp (10–15 dpf) three times daily.

For temozolomide (TMZ) treatment, TMZ (MedChemExpress) was dissolved in 10% dimethyl sulphoxide (DMSO), and the larvae at 14 dpf were treated with TMZ for 3 months at a final concentration of 100 μm/l—which does not appreciably affect the embryonic development of wild-type zebrafish (Geiger *et al.*, 2008)—and then processed for histological analysis. The tank water and TMZ were refreshed daily. The animal experiments were performed according to the protocol, and approved by Shantou University Medical College.

Synthesis of mRNA and guide RNA

Cas9 mRNA was produced by *in vitro* transcription from a pCS2 Cas9 vector (Jao *et al.*, 2013) using a mMESSAGE mMACHINE™ SP6 kit (Invitrogen, Thermo Fisher Scientific). Guide RNAs (gRNAs) were designed using the CHOPCHOP website (http://chopchop.cbu.uib.no/). The gRNA transcription templates were prepared through PCR amplification using T7-targetsite-F primers and the universal reverse primer gRNA-R (Supplementary Table 1), and gRNAs were transcribed using the MAXIscript T7 kit (Thermo Fisher Scientific). The pCS-TP vector was linearized using NotI endonuclease (New England Biolabs), cleaned up by phenol/chloroform extraction, and synthesized from linearized vectors using mMESSAGE mMACHINE™ T7 Kit (Invitrogen). All mRNA transcripts were purified using MicroElute RNA Clean-Up kit (Omega Bio-Tek). The quality and concentration of RNA were analysed by electrophoresis and NanoDrop™ 2000 spectrophotometer (Thermo Fisher Scientific). The *in vitro* efficiencies of the gRNAs were examined using a gRNA Activity Detection kit (ViewSolid Biotech).

DNA construction and microinjection

We cloned the zebrafish *U6-3* promoter (Halbig *et al.*, 2008) from the AB strain, followed by an NheI site, into the CRISPR/Cas9 skeleton vector (*Cas9-T2A-mCherry*) from the Tol2 kit (Kwan *et al.*, 2007) using ClaI and KpnI endonucleases (New England Biolabs). The sequences of gRNA were then inserted in *Cas9-T2A-mCherry,U6* to construct *Cas9-T2A-mCherry,U6:gRNA* vectors, respectively including *gfap:Cas9-T2A-mCherry,U6:gRNA(nf1a)*, *gfap:Cas9-T2A-mCherry,U6:gRNA(tp53)*, and *gfap:Cas9-T2A-mCherry,U6:gRNA(rb1)* vectors, and *gfap:Cas9-T2A-mCherry,U6:gRNA(null)* as control. Ultimately, we cleaved the *gfap* promoter from *Tg(gfap:GFP)* fish followed by *XhoI* and *AgeI* sites (Bernardos and Raymond, 2006), and subcloned the *gfap* promoter sequence into *Cas9-T2A-mCherry,U6:gRNA* vectors using T4 DNA ligase (Thermo Fisher Scientific), respectively.

The AB strains were bred and their embryos were collected for microinjection. Specifically, the mixture with 20 pg DNA construct and 20-pg *Tol2* mRNA was injected into the embryos at the one-cell stage. For typical CRISPR experiments, the mixture with 600 pg *Cas9* mRNA and 25 pg gRNA was injected into each embryo. Following microinjection, all embryos were raised in E3 medium at 28°C. The details of DNA construction and the generation and identification of tissue-specific gene mutation in zebrafish are provided in the Supplementary material.

Analysis of gRNA efficiency, T7 endonuclease I mutagenesis assay and whole-mount *in situ* hybridization

The gRNA target site and primer sequences used for the T7E1 assays are shown in Supplementary Table 1. Genomic DNA was extracted from 15 embryos using a standard DNA extraction protocol following co-microinjection of gRNA- and *Cas9*-capped RNA at 24 h post-fertilization (hpf). PCR mixtures were then prepared using the TransFast® Taq DNA polymerase (TransGen Biotech). PCR products (8.5 μl) were then annealed for heteroduplex formation. T7 endonuclease I buffer (1 μl) and 0.5 ml T7 endonuclease I (ViewSolid Biotech) were added to the solution described above, and the mixture was incubated at 37°C for 25 min. The samples were analysed using 2% agarose gels and observed with a gel imaging system (Junyi). To confirm the efficiency of gRNAs, 2 ml of PCR products was cloned into the pMD-19T vector (Takara Bio) for DNA sequencing.

Whole-mount *in situ* hybridization assay of *tp53*, *nf1a* or *rb1* was performed as previously described (Padmanabhan *et al.*, 2009). The sense and antisense RNA probes were synthesized using the mMESSAGE mMACHINE™ T7 Kit (Invitrogen). *In situ* hybridization was carried out following the previous protocol (Thisse and Thisse, 2008).

Histological examination, immunohistochemistry, immunofluorescence and whole-mount embryonic imaging

The whole brain tissue specimens from the euthanized transgenic zebrafish were dissected, paraformaldehyde-fixed, and paraffin-embedded for haematoxylin and eosin staining and immunohistochemistry. The immunohistochemistry of formalin-fixed, paraffin-embedded tissue sections was carried out as previously described (Barash *et al.*, 2019). Following antigen retrieval and blocking, 4-mm sections were immunostained using the primary antibodies and the corresponding secondary antibodies, and were detected using the avidin-biotin complex method (Dako), and visualized with DAB. The slides were

lightly counterstained with haematoxylin, and the staining was evaluated with Image-Pro Plus software (Media Cybernetics Inc.). The paraffin-embedded tissue microarray of human glioma specimens was purchased from Outdo Biotech Ltd (HbraG180Su01). The ethics approval was approved by the Medical Ethics Committee of Shantou University Medical College.

The glioma formation developed by the fish was preliminarily estimated based on the 'bending-body' phenotype before post-mortem histological analysis, and confirmed by haematoxylin and eosin staining. The histological grades varied from I to IV of brain harboured gliomas and were further diagnosed by the pathologist according to the WHO classification and as previously described (Jung *et al.*, 2013; Villa *et al.*, 2018). For example, advanced histological grade glioma is usually accompanied by larger tumours, hypercellularity, enhanced necrosis and vascularity, and frequent mitosis, as well as robust expression of gliomagenesis-related factors, including Gfap, Pcna, phh3, pAkt, and Nestin.

Immunofluorescence was performed using 25-mm cryosections of 4% paraformaldehyde-fixed tissues as previously described (Luo *et al.*, 2018). The sections were incubated overnight at 4°C with the primary antibodies in blocking buffer. The sections were then washed six times with PBS containing 0.5% Triton™ X-100 at room temperature for 15 min, incubated with the secondary antibodies at room temperature for 1 h, washed with PBS, and sealed with coverslips. The immunostained sections were observed and photographed under a confocal microscope (FV1000; Olympus). The whole-embryonic fluorescent images were obtained using an Olympus MVX10 fluorescence microscope. All information on the antibodies and the concentrations used are provided in Supplementary Table 2.

Quantitative RT-PCR assay

The dissected brain tissues from 3-month-old fish were used for quantitative PCR. Samples were collected from three or four fish belonging to each group, and used for total RNA extraction with TRIzol™ reagent (Invitrogen). The extracted RNA was reverse-transcribed by qRT-PCR assay using QuantiTect™ SYBR Green PCR kit (Qiagen), and amplified by 7300 Real-time PCR System (Applied Biosystems). All experiments were performed three times using separately prepared samples. The sequences of the primers used in qRT-RCR assay are provided in Supplementary Table 1.

Western blot analysis

The dissected brain tissues from 3-month-old fish were lysed in RIPA buffer containing 1% PMSF (Solarbio). Samples were collected from three or four fish, separated with electrophoresis, and transferred to nitrocellulose membranes (Millipore). The membranes were incubated with 5% bovine serum albumin (BSA) in Tris-based saline-Tween 20 (TBST; 0.2 M Tris, 1.37 M NaCl, and 0.1% Tween 20 at pH 7.6), and the primary antibodies at 4°C overnight. After washing with TBST, the membranes were then incubated with the secondary antibodies, and visualized using a SuperSignal™ West Pico Substrate Kit (Thermo Fisher Scientific). All the experiments were repeated independently three times. All the information on the antibodies and the utilized concentrations are provided in Supplementary Table 2.

Global transcriptome sequencing and analyses

Total RNA from each group was isolated using the TRIzol™ reagent, and sequenced by BGI Company. Unsupervised hierarchical clustering (UHC) analyses were performed to calculate the median absolute deviation score for each probe set using the $\log_2$-transformed data, and the top 1000 most variable probe sets were selected. The analysis was performed using GeneMaths software (Applied Maths, Inc., Austin, TX) with Pearson correlation as the similarity coefficient and Ward as the clustering method.

The enrichment of signature genes in the tumour subgroups identified by UHC in our models was assessed by gene set enrichment analysis (GSEA) (Subramanian *et al.*, 2005). We generated gene sets using the gene signatures that define previously identified glioma subgroups (Freije *et al.*, 2004; Phillips *et al.*, 2006; Verhaak *et al.*, 2010), and performed GSEA analysis of tumours to compare one subgroup with the other two subgroups. A nominal P-value of <0.2 obtained in GSEA was considered to indicate statistical significance.

Behavioural tests

The motor capabilities of the larvae in different groups were evaluated using a behavioural tracking system (Noldus). In each trial, the 7 dpf larvae of different experimental groups were carefully transferred to a 24-well plate with one single larva in each well. The plate was placed into an observation chamber, the swim path of individual larvae was recorded with an infrared video camera for 6.5 min, and the travelling distance of each larva was analysed using DanioVision software (Noldus). Briefly, basal activity in the darkened chamber was recorded for 30 s, followed by a 0.2-s exposure to a 500-lx white light stimulus, and repeated the next 30 s in the dark. DanioVision software quantified larval motor activity by assessing changes in infrared image pixel intensity (on a scale of 1 to 256) of all pixels corresponding to the image area of its circular well between sequential video sweeps (every 40 ms).

Quantification and statistical analysis

The results were analysed using SPSS 10.0 statistical software (SPSS, Chicago, IL), and presented as the arithmetic means and standard error (SE). Student's t-test was used for the statistical analyses. $P < 0.05$ was regarded as indicating statistical significance.

Data availability

All sequencing that support the findings of this study have been deposited in the Gene Expression Omnibus (GEO) of National Center for Biotechnology Information under accession no. GSE129899.

Results

The generation and identification of tissue-specific *nf1*, *rb1* or *tp53*-deficient zebrafish

Based on CRISPR/Cas9 technology (Ablain *et al.*, 2015), a vector framework (*Cas9-T2A-mCherry,gRNA*) was inserted with two key promoters: one was the zebrafish *U6-3* promoter, which can drive the expression of the targeting gRNA (Halbig *et al.*, 2008), and the other was zebrafish *gfap* regulatory elements (Bernardos and Raymond, 2006), which tissue-specifically control the expression of zebrafish codon-optimized Cas9 and the fluorescent reporter mCherry (Fig. 1A). Thus, the *gfap*:*Cas9-T2A-mCherry,U6*:*gRNA*(*null*) vector (the vector with a null gRNA target as the control, and the corresponding fish line is named $gfap^{WT}$) allows the identification of Cas9-expressing cells in zebrafish through examining the concomitant mCherry expression.

It was known that there are two closely related zebrafish orthologues, *nf1a* and *nf1b*, with highly homologous, sharing 57 exons and similar genomic structures. The mutation of *nf1a*, *nf1b*, or both together displays similar defective phenotypes in *Nf1*-deficent mouse embryos (Padmanabhan *et al.*, 2009). We identified a homologous target gene from the first exons of *nf1a*, which is also the identical target sequence of *nf1b*, to eliminate the expression of Nf1a, and potentially knock down Nf1b expression in zebrafish (Supplementary Fig. 1A). When injected with *Cas9* mRNA into single-cell zebrafish embryos, the T7E1 assay (Kim *et al.*, 2009) showed the effectiveness of *nf1a*, *rb1* and *tp53* gRNAs (Supplementary Fig. 1B), and these target sequences (Supplementary Fig. 1C) were then cloned into the *gfap*:*Cas9-T2A-mCherry,U6*:*gRNA*(*null*) vector to construct the CRISPR vector [*gfap*:*Cas9-T2A-mCherry,U6*:*gRNA*(*nf1a*, *rb1*, or *tp53*) vectors], respectively.

Transgenic fish lines were generated by microinjecting the CRISPR vector and *Tol2* transposase mRNA, which can be translated into active transposase in embryonic cells, to catalyse the integration of the vector into the zebrafish genome within a short period of time (Fig. 1B). We observed the vector randomly integrated into a subset of embryonic cells and subsequently generated mosaic Cas9- and mCherry-expressing embryos at 3 dpf in founder fish (Supplementary Fig. 1D), and their offspring with germ-line transmission can be easily identified by the stable expression of mCherry in neurogliocytes (Fig. 1C). To determine the localization of mCherry-labelled Cas9 and endogenous Gfap, we crossed $gfap^{WT}$ and *Tg*(*gfap*:*GFP*) transgenic fish, which labelled endogenous Gfap with GFP reporter in zebrafish (Bernardos and Raymond, 2006). The results indicated that the expression patterning of mCherry-labelled Cas9 and GFP-labelled endogenous Gfap was exactly co-localized in either brain or spinal cord in their 60 hpf offspring (Fig. 1D). In addition, confocal microscopy and *in situ* hybridization indicated the identical co-localization between endogenous Gfap and mCherry in the tissues of retina (Fig. 1E–G) and spinal cord (Fig. 1H–J), as well as similar tissue-restricted expression pattern of Cas9 in CNS (arrowheads; Fig. 1K) of F_1 $gfap^{WT}$ larvae at 48 hpf, suggesting that mCherry was concomitantly expressed with *gfap* promoter-driving *Cas9* in zebrafish.

We next selected the larvae with the typical phenotype that expressed faithful and robust fluorescence in the brain as the parent to obtain the F_1 $gfap^{Cas9\text{-}mCherry}$;*nf1a* (*nf1* KO), $gfap^{Cas9\text{-}mCherry}$;*rb1* (*rb1* KO), and $gfap^{Cas9\text{-}mCherry}$;*tp53* (*tp53* KO) fish lines, respectively. There were four phenotypic types with different mCherry expression patterning (types 1, 2, 3 and 4) in all three single mutants and $gfap^{WT}$ control in F_1 generation (Supplementary Fig. 1E). We selected the fish lines with the type 2 phenotype, which mCherry-labelled Cas9 strictly expressed in brain and spinal cord, and outcrossed with wild-type fish to obtain the F_2 generations of *nf1* KO, *rb1* KO, *tp53* KO fish lines, and $gfap^{WT}$ control, respectively. We then performed the T7E1 mutagenesis assay to identify the mutations of targeting genes in transgenic zebrafish. The results indicated the definitive mutation at the target locus in the brains that was only detected with vectors containing specific gRNA, including *nf1a*, *rb1* and *tp53* (Supplementary Fig. 2A). Meanwhile, PCR amplicons of the targeted loci were sequenced to quantitatively measure the mutation efficiency. The results showed that the frameshift mutations were detected in >60% fish (Supplementary Fig. 2B and Supplementary Table 3), indicating that the mutations in brains were efficiently generated in *nf1* KO, *rb1* KO, and *tp53* KO fish, respectively. Similarly, the whole-mount *in situ* hybridization showed the mRNA level of *Nf1a*, *Rb1*, or *Tp53* was almost undetectable in these KO larvae (Supplementary Fig. 2C).

The stable F_3 homozygous strains, including all three *nf1* KO, *rb1* KO, and *tp53* KO fish lines, were ultimately obtained from the in-cross of these F_2 generation KO lines, preliminarily identified using the determination of fluorescent intensity at 3 dpf, and confirmed using the cutting-tail method and T7E1 assay at 30 dpf (Supplementary material). Immunofluorescence showed that the co-localization between *gfap* promoter-driving mCherry expression and endogenous Nf1, Rb, or Tp53 expression was totally undetected in *nf1* KO, *rb1* KO, or *tp53* KO adult fish at 3 months of age (arrowheads; Fig. 2A), whereas mCherry expression co-localized with the expression of these specific endogenous genes in $gfap^{WT}$ fish (Fig. 2A, arrows), indicating that the expression of Nf1, Rb1 or Tp53 was specifically disrupted based on the concomitant *gfap*

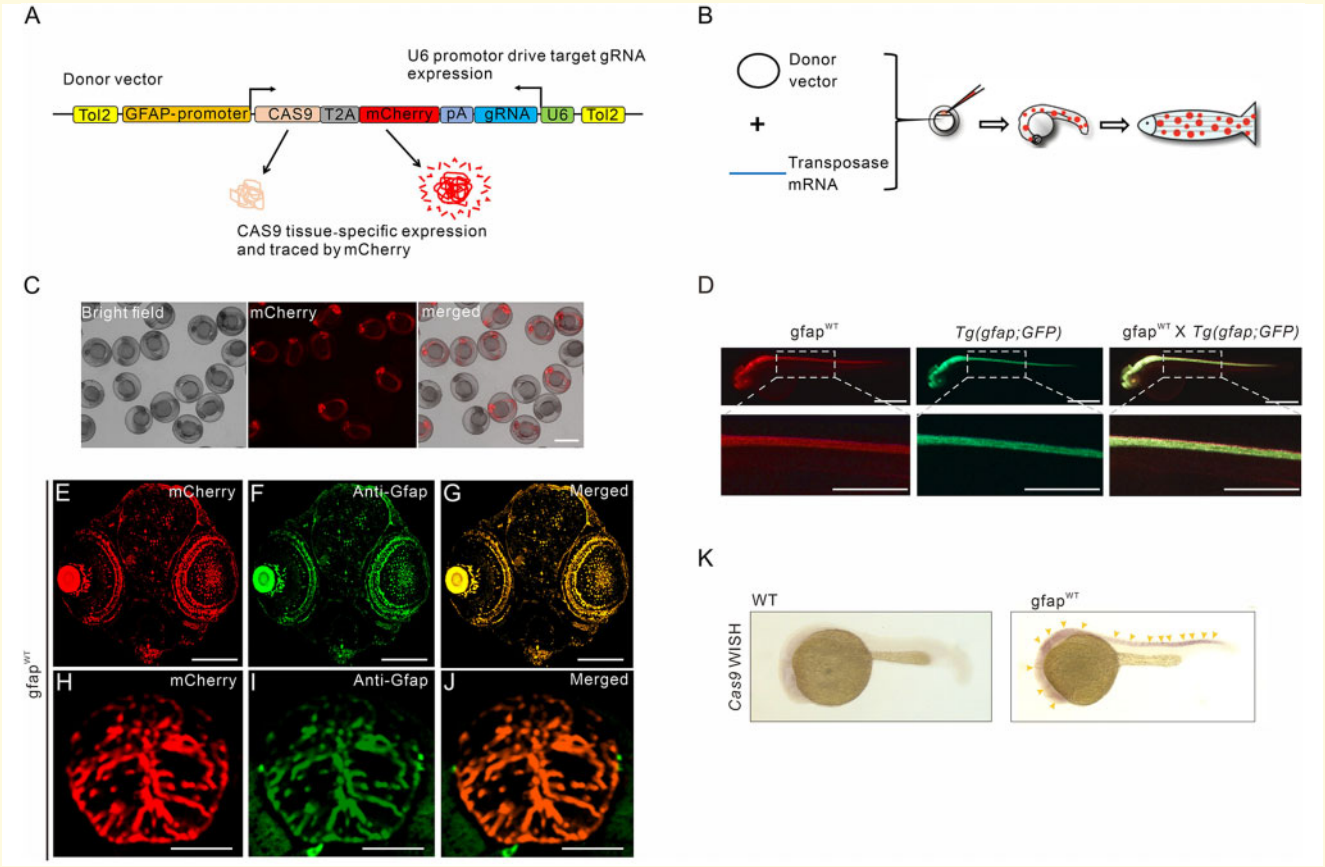

Figure 1 CRISPR/Cas9-based deletion system in zebrafish. (**A**) Schematic illustration of the constructs of the CRISPR/Cas9-based vector, including the *gfap* promoter-driving Cas9, mCherry reporter, and U6-driving specific gRNA. (**B**) Strategy of the generation of the transgenic zebrafish lines. (**C**) F_1 transgenic fish generated by mosaic mCherry-positive fish outcrossed with wild-type fish. A subset of the transgenic offspring was identified by mCherry-positive astrocytes. Scale bar = 1 mm. (**D**) The colocalization of mCherry-labelled Cas9 and GFP-labelled endogenous Gfap in 60 hpf offspring from the cross of $gfap^{WT}$ and *Tg*(*gfap*:*GFP*) transgenic fish. Scale bars = 500 μm. (**E**–**J**) Co-localization of mCherry fluorescent signals (red) and endogenous Gfap detected by anti-Gfap antibody (FITC; green) in the brain and retina (**E**–**G**) or spinal cord (**H**–**J**) tissue. Scale bars = 200 μm. (**K**) Representative images of whole-mount *in situ* hybridization using an anti-sense RNA probe against Cas9 mRNA in 48 hpf embryos injected with *Tol2* mRNA and *gfap:Cas9-T2A-mCherry,U6:gRNA*(*null*) vector expressing Cas9 under the control of the *gfap* promoter. Cas9 expression pattern is governed by the tissue-specificity of *gfap* promoter (yellow arrowheads). Scale bars = 500 μm.

promoter-driving Cas9 in zebrafish neurogliocytes. It is noted that the total expression of Nf1a and Nf1b, which can be simultaneously recognized by the anti-Nf1 antibody, were significantly inhibited in *nf1* KO brains of adult fish (Supplementary Fig. 2D). Also, further investigations confirmed the inhibition of Nf1, Rb1, or Tp53 in the brain tissues of these fish lines (Supplementary Fig. 2D–F). In 3-month-old adult $gfap^{WT}$ fish, mCherry expression was detected in the dorsum of the cerebellum and medulla in brain tissue (Fig. 2B). The precise mCherry expression patterns in different sections of adult $gfap^{WT}$ fish (Fig. 2B, green dashed lines) are shown in Fig. 2C, where mCherry-labelled Gfap expression (red signal) was particularly robust in cells along the midline of the cerebellum and at the intermediate layer and ventricular zone (dorsal lining of the fourth ventricle) in adult $gfap^{WT}$ fish (Fig. 2C). Thus, this evidence suggests that the Nf1, Rb1, or Tp53 pathway was efficiently blocked in CNS tissue at embryonic and adult developmental stages in zebrafish.

Targeted mutagenesis of *nf1*, but not *rb1* or *tp53*, initiates gliomagenesis in the mature brain tissue of zebrafish

To investigate the effects of *nf1* mutation in mature radial glia, we first examined the expression of Nf1 and Gfap in the brain tissues of *nf1* KO fish. The results indicated endogenous Nf1 expression was significantly inhibited, whereas Gfap expression was upregulated in the brain tissues of *nf1* KO and $gfap^{WT}$ fish (Fig. 3A and Supplementary Fig. 2G). Additionally, we found a morphological disruption, the 'bending-body' phenotype, which was initially detected in

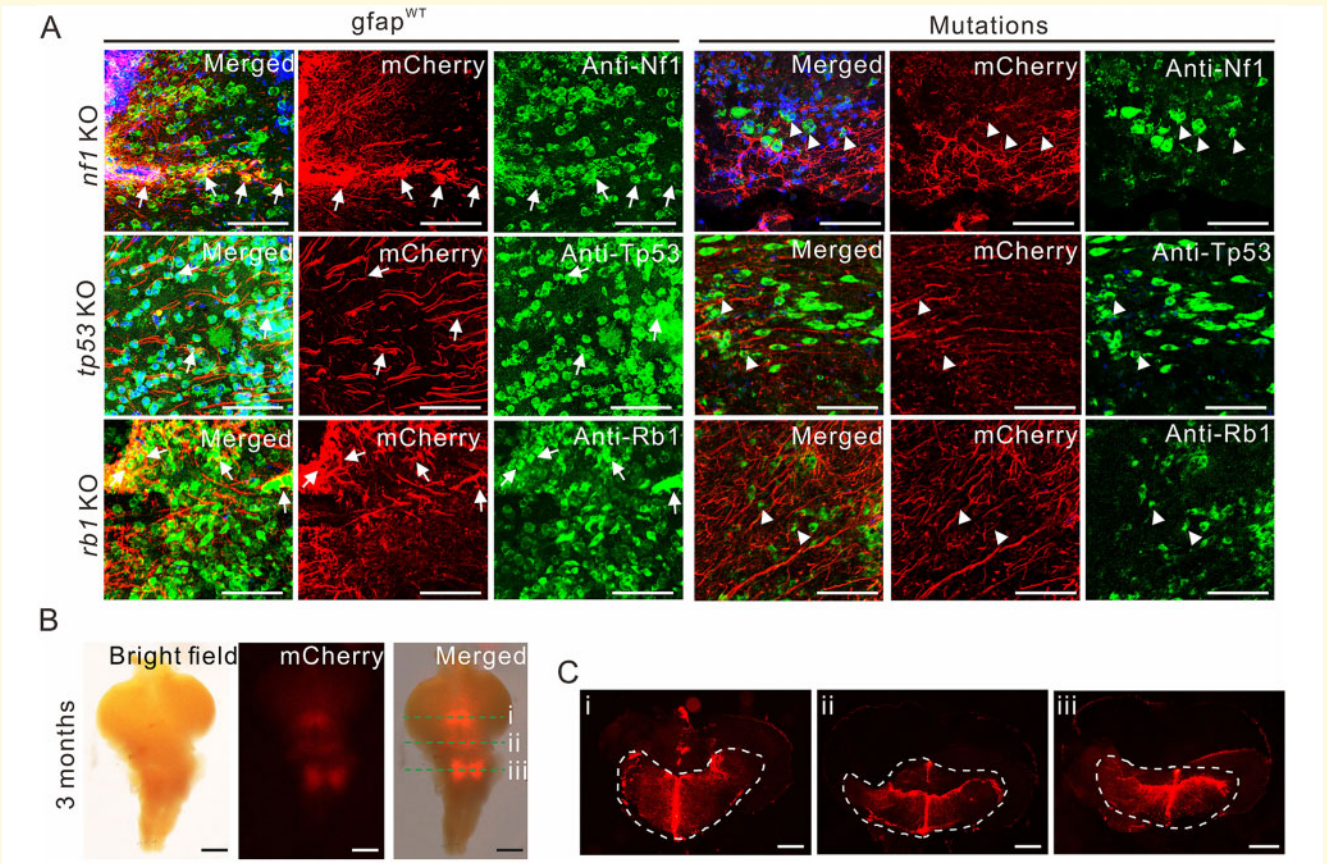

Figure 2 Disruption of tissue-specific genes in larvae and adult zebrafish. (**A**) Representative images of various single-deletion mutations, and *gfap*^{WT} control in 3-month-old adult fish. The fluorescent radial glia phenotype was observed based on mCherry-labelled Gfap expression, which failed to co-localize with Nf1, Rb1 or Tp53 expression in brain tissues of transgenic zebrafish (arrowheads; *right*), whereas partial co-localizations of mCherry-labelled Gfap with Nf1, Rb1 or Tp53 expression were observed in *gfap*^{WT} fish (arrows; *left*). Scale bars = 50 μm. (**B**) Merged bright and fluorescent images showing mCherry-labelled Gfap expression in the cerebellum and medulla in 3-month-old *gfap*^{WT} fish. Scale bars = 500 μm. (**C**) Coronal sections of the images shown in **i–iii**. Robust mCherry-labelled Gfap expression was observed along the midline and dorsal lining of the fourth ventricle. Scale bars = 50 μm.

2-month-old *nf1* KO fish (Fig. 3B). We expected that the process through which the body became bent and gradually tortuous might be positively associated with brain tissue disruption, which appears to be attributable to motor disturbances caused by glioma formation in the cerebellum (Jung *et al.*, 2013). Since the 'bending-body' phenotype is always coupled with the appearance of glioma formation, we therefore hypothesized that it might be a surrogate marker of gliomagenesis in zebrafish. Compared with the *gfap*^{WT} control, we did not observe any developmental disruption in the spinal cord in 2-month-old *nf1* KO fish with the bended phenotype (Fig. 3B). In contrast, the brain tissues dissected from the fish with 'bending-body' phenotype displayed the brain architecture disruption in *nf1* KO fish [Fig. 3C(i and v)], which has the gradually increasing tumour incidence and mortality rates in a time-dependent manner (Supplementary Fig. 2H and I). Further histological examination demonstrated a range of histopathological features in brain tissues of 3-month-old *nf1* KO fish with the 'bending-body' phenotype. The results revealed that the tumours in the periventricular area showed tumour invasion into the fourth ventricle [Fig. 3C(vi), arrowheads]. Moreover, we noticed that some areas were more pleomorphic with enlarged and hyperchromatic nuclei [Fig. 3C(vii and viii), broken line], which indicated tumour formation in the periventricular area in *nf1* KO fish.

Immunohistochemistry demonstrated the moderately upregulated expression of several gliomagenesis-related proteins in 3-month-old *nf1* KO fish (Fig. 3D). For example, the cells in the ventricular lining and intermediate layer of the tumours derived from the brain tissue of *nf1* KO fish slightly showed immunoreactivity to proliferative markers (Pcna). The results also showed positive staining for phosphohistone H3 (pHH3), a mitotic marker, indicating that the generated tumour exhibited high proliferative mitotic activity. Meanwhile, the modestly increasing phosphorylated Akt (pAkt) expression, and the significant upregulation of Gfap, a classic astrocytic marker, in the tumours generated from *nf1* KO fish, suggested the presence of highly proliferative radial glia. In addition, our results also showed cyclin D1

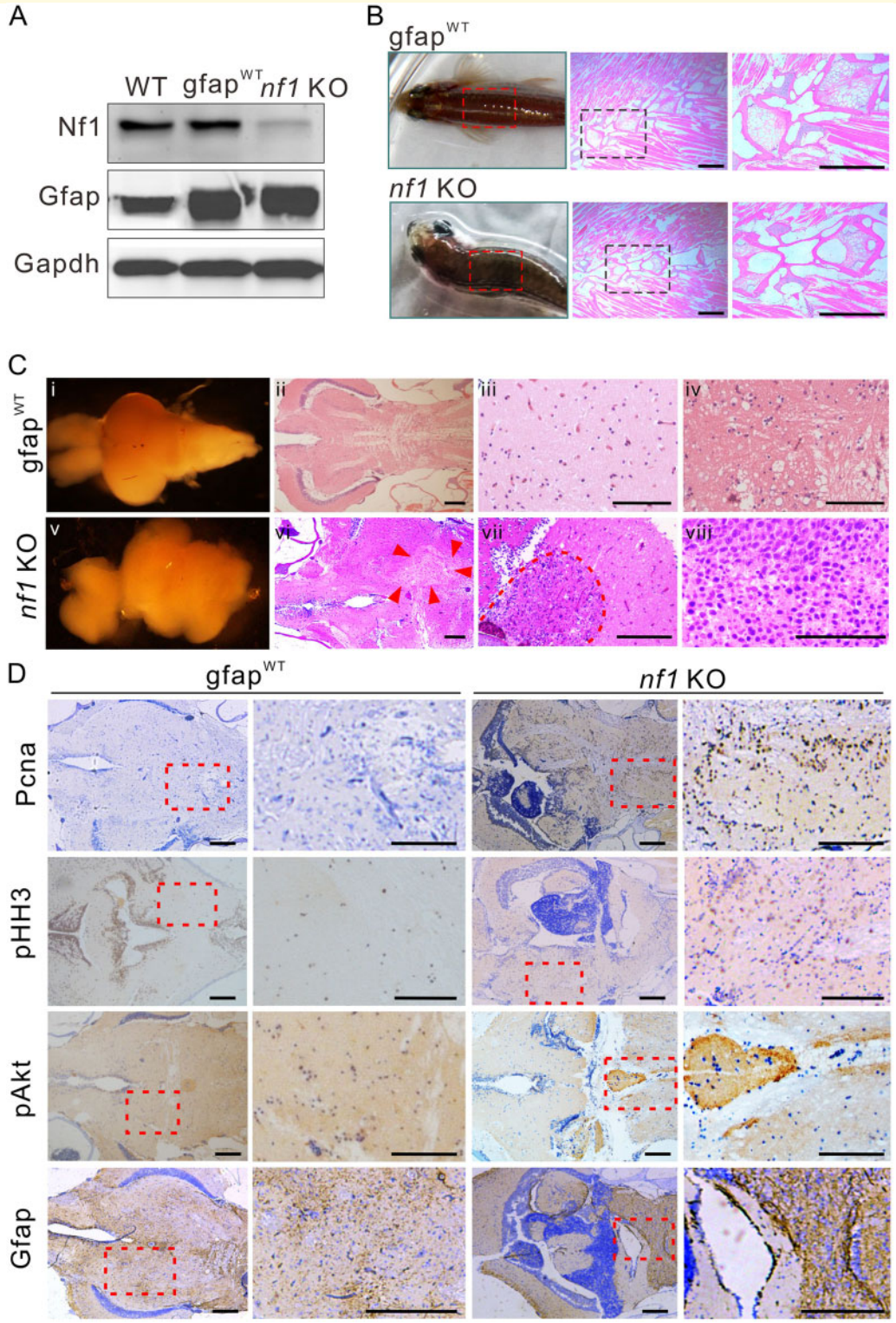

Figure 3 Nf1 mutagenesis in radial glia disrupts the brain architecture and initiates gliomagenesis. (**A**) Western blot determination of Nf1 and Gfap in brain tissues from wild-type, *gfap*^{WT}, and *nf1* KO fish ($n = 3$). (**B**) Typical 'bending-body' phenotype and haematoxylin and eosin staining of spinal cord tissue in 2-month-old transgenic zebrafish. Scale bars = 50 μm. (**C**) The architectures and histology of brain tissues from 3-month-old *gfap*^{WT} and *nf1* KO fish. Brain architecture of 3-month-old *gfap*^{WT} (**i**) and *nf1* KO fish (**v**). (**ii**–**iv**) Haematoxylin and eosin staining of the cerebellum of *gfap*^{WT} fish. (**vi**–**viii**) The tumours that formed throughout the cerebellum (at different magnifications, the boundaries were indicated by arrowheads or broken line). Scale bars = 100 μm. (**D**) Immunohistochemistry staining (*left*) and higher magnifications (*right*) of Pcna, pHH3, pAkt, and Gfap in brain tissues of 3-month-old *gfap*^{WT} and *nf1* KO fish. Scale bars = 100 μm. Data shown as mean ± SEM. $^{**}P < 0.01$, $^{***}P < 0.001$.

and β-catenin expression, which is positively correlated with gliomagenesis, were increased in *nf1* KO fish (Supplementary Fig. 2J). Notably, the typical phenotype of hyperproliferation, hypertrophy, or abnormal multinucleated glial cells, which is linked to glioma development and progression, was seldomly observed in the brain tissue of *nf1* KO fish, suggesting that *nf1* mutation alone in glial cells mainly induces low-grade glioma, which potentially reflects lower tumour incidences in 3- and 6-month-old *nf1* KO fish (11% and 19%) (Fig. 5D and Supplementary Table 4). Furthermore, we did not observe any tumour formation in the brain tissues from *rb1* KO ($n = 41$) and *tp53* KO ($n = 37$) fish until 6 months of age (Fig. 5E), suggesting that only the single mutation of *nf1*, but not *rb1* or *tp53*, can initiate gliomagenesis in zebrafish.

Tp53 mutation accelerates the development of glioma in *nf1* or *rb1* knockout fish

To gain insight into the cooperation among the Nf1, Tp53, and Rb1 signals in gliomagenesis in zebrafish, the homozygous *nf1*;*tp53* combined KO (cKO), *nf1*;*rb1* cKO, and *tp53*;*rb1* cKO fish lines, were generated and identified from the cross of F_3 generation *nf1* KO, *tp53* KO, and *rb1* KO fish, respectively. In addition to the bended phenotype, the visible bump was also observed on the heads of some 2- and 3-month-old *nf1*;*tp53* cKO fish [Fig. 4A(i, vii and xiii)]. Histological examination revealed that the tumours generated from *nf1*;*tp53* cKO fish were invariably located near the fourth ventricle, resulting in the disruption of the ventricular lining and a space-occupying mass in the ventricle of brain tissue. Compared with the brain tissues of $gfap^{WT}$ fish [Fig. 4A(i–vi)], the histological features of adult *nf1*;*tp53* cKO fish showed glioblastoma multiforme [Fig. 4A(viii and ix)], increasing number of multinucleated glial cells [Fig. 4A(xi and xvi), arrowheads], necrosis [Fig. 4A(xiv and xv)], frequent vascularity [Fig. 4A(xii and xviii), arrowheads], enhanced invasive capability [Fig. 4A(x), broken line], and typical gliomatosis phenotype [Fig. 4A(xvii)]. It is noted that the tumours derived from *nf1*;*tp53* cKO fish gradually generated in the whole cerebellum, invaded the midbrain, and showed histological grades due to the presence of intratumoral cell nests with the increasing cellularity, which further revealed by an increasing reactivity to proliferative markers and relevant tumour indicators. The results indicated that the expression levels of several gliomagenesis-relevant effectors, including pAkt, Pcna, pHH3, Gfap, β-catenin, as well as Nestin, key markers of cancer stem cells in malignant tumours (Brustle and McKay, 1995), were dramatically increased in brain tissues of 2- and 3-month-old *nf1*;*tp53* cKO fish (Fig. 4B and C).

Similar gliomatosis phenotypes, including the increasing number of multinucleated radial glia, enhanced necrosis and vascularity, and greater hypercellular areas, were observed in 3-month-old *rb1*;*tp53* cKO fish (Fig. 5A). In addition, the expression of gliomagenesis-relevant factors, such as Gfap, Pcna, pHH3, and pAkt, was also significantly upregulated in brain tissue of *rb1*;*tp53* cKO fish (Fig. 5A). In this context, the survival rates of *rb1*;*tp53* cKO and *nf1*;*tp53* cKO fish (72% and 47%) were lower than *nf1* KO fish (87%) at 6 months, respectively ($n = 100$ for each group) (Fig. 5B, Supplementary Fig. 2I and Supplementary Table 4). Meanwhile, histological examination revealed that the cancer incident rates in *rb1*;*tp53* cKO and *nf1*;*tp53* cKO fish (44% and 67%) were higher than *nf1* KO fish (19%) at 6 months ($n = 100$ for each group) (Fig. 5C, Supplementary Fig. 2H and Supplementary Table 4). In the gliomas generated from the brain tissue in zebrafish, further pathological analyses demonstrated that the proportions of malignant gliomas (grade III or IV) in *rb1*;*tp53* cKO and *nf1*;*tp53* cKO fish (18/30 and 24/30) were much higher than those in *nf1*;*rb1* cKO and *nf1* KO fish (10/30 and 8/30) at 6 months (Fig. 5D). These findings indicated that the additional *tp53* mutation strongly promotes gliomagenesis in *nf1* KO and *rb1* KO fish by increasing tumour incidence and malignant grades in a time-dependent manner.

Notably, the proportions of malignant gliomas in the tumours derived from *nf1*;*rb1* cKO fish were nearly equal to those found in *nf1* KO fish, and significantly lower than those in *rb1*;*tp53* and *nf1*;*tp53* cKO fish (Fig. 5D). Additionally, similar histological phenotypes (Fig. 3C and Supplementary Fig. 3A) and immunoreactivities (Fig. 3D and Supplementary Fig. 3B) were observed in *nf1* KO and *nf1*;*rb1* cKO fish, suggesting that *rb1* ablation may be less effective than *tp53* mutation for glioma development in the absence of Nf1 in zebrafish. Thereafter, we characterized the main features, including survival rate, tumour incidence, and tumour malignancy, of the 6-month-old fish with the various mutations (Fig. 5E). Gradual increases in tumour incidence and malignant grades were observed in *nf1* KO, *nf1*;*rb1*, *rb1*;*tp53*, and *nf1*;*tp53* cKO fish, whereas tumour incidence was undetected in $gfap^{WT}$, *rb1* KO, and *tp53* KO zebrafish within the first 6 months of age.

Developmental disruption in *nf1*;*rb1*;*tp53* triple combined knockout zebrafish

We then investigated the effects of the concurrent dysregulation of the RTK/Ras/PI3K, Tp53, and Rb1 pathways in zebrafish (Cancer Genome Atlas Research, 2008; Ethan *et al.*, 2010). The heterozygous *tp53*;*nf1*;*rb1* triple cKO (triple cKO) fish line was generated from the cross of the homozygous *nf1*;*rb1* cKO and *tp53* KO fish lines. Notably, most heterozygous triple cKO embryos (>80%) displayed severe developmental disruption, including altered organization of somites, and the bending of the anterio-posterior axis in

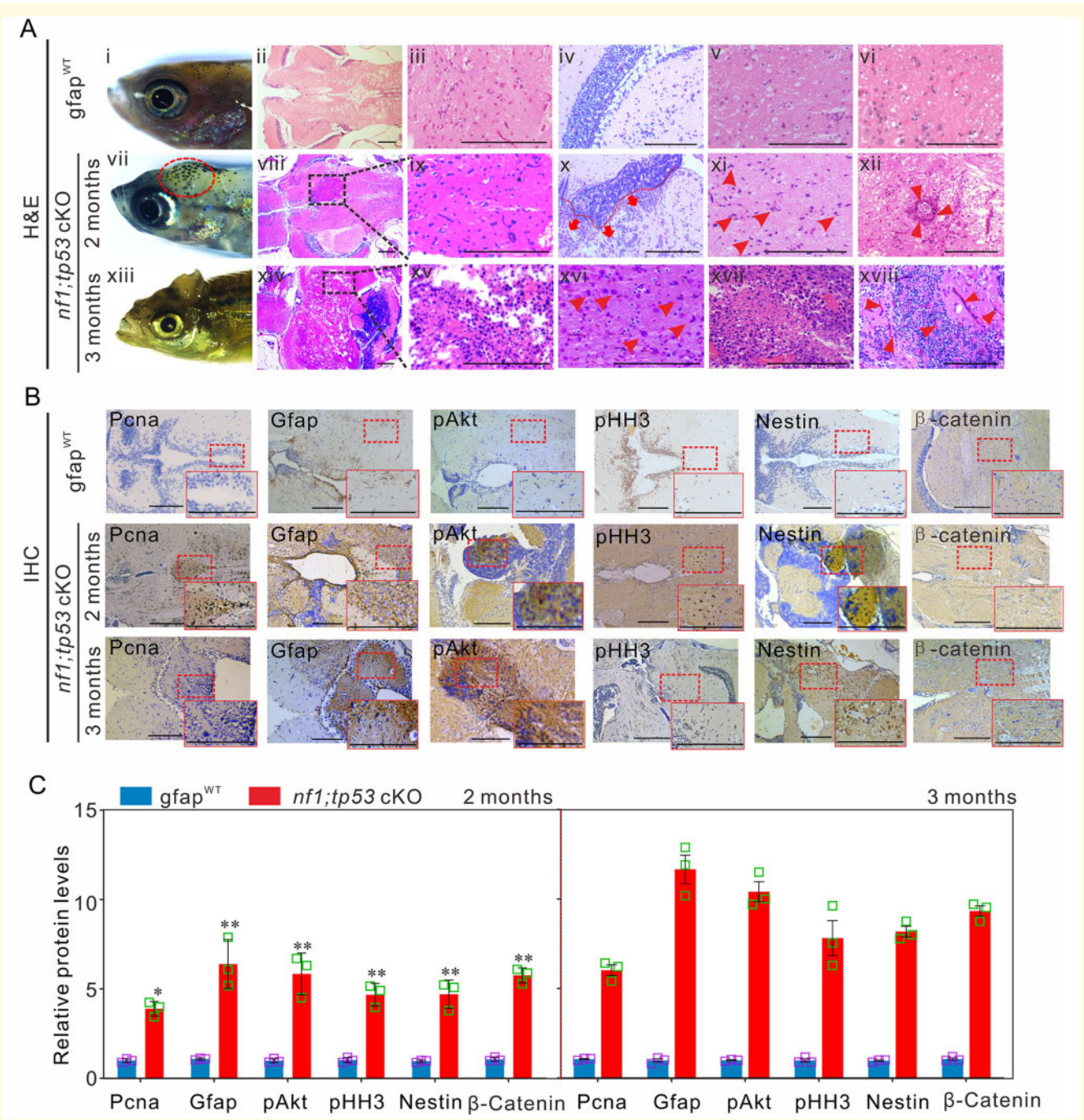

Figure 4 *Tp53* mutation promotes the development of gliomagenesis in zebrafish. (**A**) Histological examinations of 2-month-old *gfap*^{WT} and *nf1*;*tp53* cKO fish, and 3-month-old *nf1*;*tp53* cKO fish. (**i**, **vii** and **xiii**) Representative images of the bumps on the heads of *nf1*;*tp53* cKO fish. (**ii**–**vi**) Representative images of haematoxylin and eosin (H&E) staining of normal brain tissues of *gfap*^{WT} fish. Several typical gliomagenic phenotypes, including glioblastoma multiforme (**viii** and **ix**), increased numbers of multinucleated glial cells (arrowheads; **xi** and **xvi**), necrosis (**xiv** and **xv**), frequent vascularity (arrowheads; **xii** and **xviii**), enhanced invasive capability (red broken line; x), and the typical gliomatosis phenotype (**xvii**), were detected in 2- and 3-month-old *nf1*;*tp53* cKO fish. (**B**) Immunohistochemistry staining was performed to examine the expression of tumour-relevant factors in brain tissues of 2-month-old *gfap*^{WT}, *nf1*;*tp53* cKO, and 3-month-old *nf1*;*tp53* cKO fish. (**C**) Quantification of immunohistochemistry staining evaluated the expression of Pcna, Gfap, pAkt, pHH3, Nestin, and β-catenin in 2- or 3-month-old *gfap*^{WT} and *nf1*;*tp53* cKO fish (n = 3 for each group). Scale bars = 100 μm. Data shown as mean ± SEM. *$P < 0.05$, **$P < 0.01$, ***$P < 0.001$.

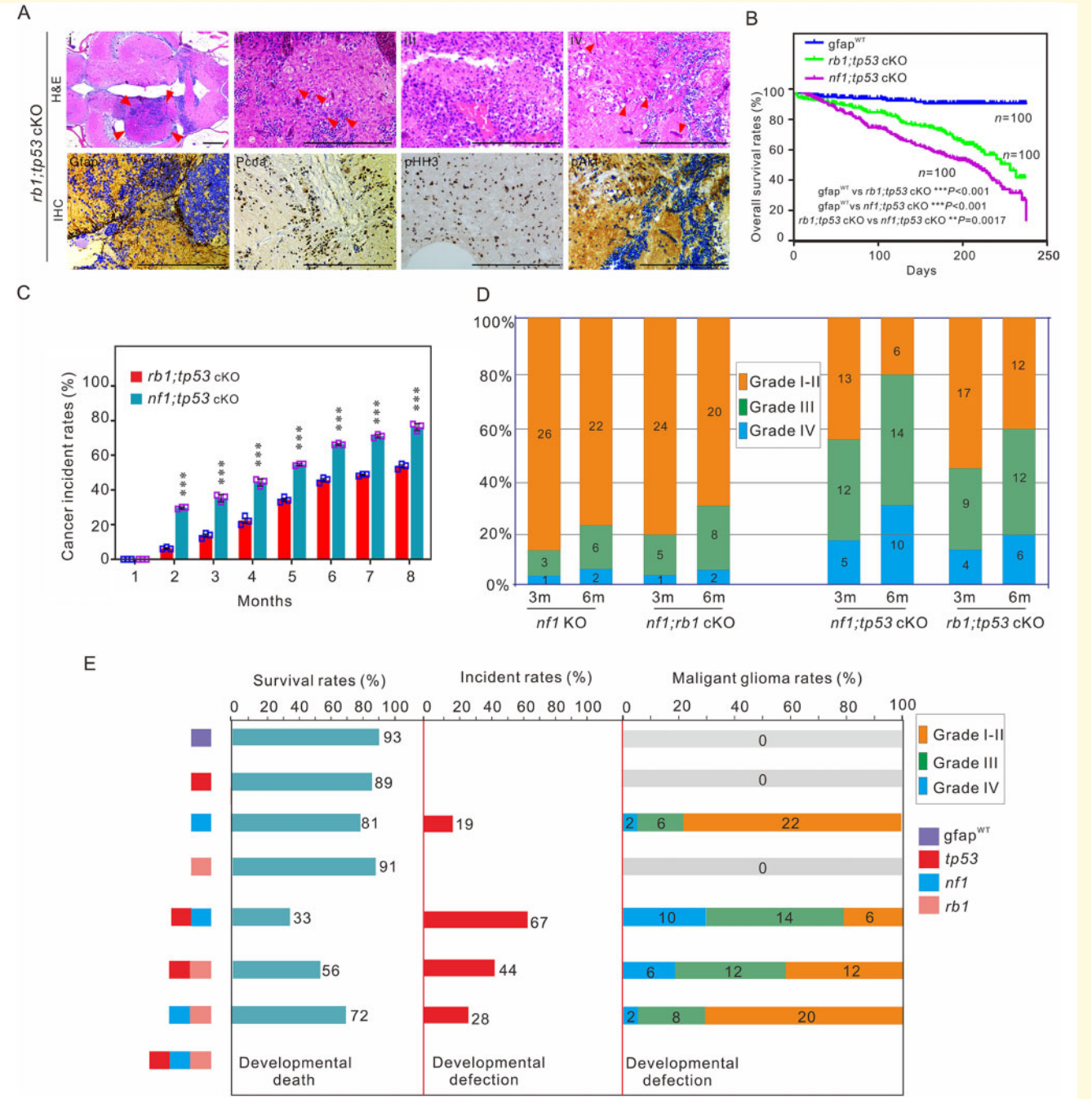

Figure 5 Tp53 mutation is critical for poor prognosis in zebrafish. (**A**) Histological examination of gliomas in 3-month-old *rb1*;*tp53* cKO fish. (**i**–**iv**) Haematoxylin and eosin (H&E) staining showed the generated tumours (arrowheads; **i**), multinucleated giant cells (arrowheads; **ii**), the typical gliomatosis phenotype (**iii**), and vascularity (arrowheads; **iv**). Immunohistochemistry staining was performed to examine tumour-relevant indicators, including Gfap, Pcna, pHH3, and pAkt, in brain tissues of *rb1*;*tp53* cKO fish. Scale bars = 100 μm. (**B** and **C**) Overall survival rates and cancer incidences of *rb1*;*tp53* cKO and *nf1*;*tp53* cKO fish, respectively (n = 100 for each group). The glioma formation was preliminarily estimated based on the 'bending-body' phenotype, and confirmed by haematoxylin and eosin staining. (**D**) Malignancy of the tumours derived from the fish with various mutations at 3 or 6 months of age (n = 30 for each group). (**E**) Summary of the survival rates, cancer incidences, and malignancy of the generated gliomas in fish lines with various mutations at 6 months of age. Data shown as mean ± SEM. ***$P < 0.001$.

spinal cord during the early developmental stage (Supplementary Fig. 4A). Additionally, in single/double mutant(s), the 'bending-body' phenotype was initially observed at 2 months (Fig. 3B), whereas the developmental disruption in spinal cord occurred in triple cKO fish at the early developmental stage (Supplementary Fig. 4A), suggesting that the 'bending-body' phenotype in single and double mutants (Fig. 3B) might not be associated with the

phenotypic alteration in spinal cord in triple mutants in zebrafish (Supplementary Fig. 4A). Moreover, the survival rate of triple cKO fish was much lower than for other transgenic fish lines (Fig. 5B and Supplementary Figs 2I and 4B), suggesting other biological events might occur in the simultaneous mutations of these three genes in astrocytes, which likely result in severely developmental disruption and malformation-related death prior to gliomagenesis (Supplementary Fig. 4B).

Interestingly, the behaviour tests of *gfap*^{WT}, *nf1* KO, *nf1*;*tp53*, and triple cKO larvae indicated significant differences in the travelling distances (Supplementary Fig. 4C) and trajectories (Supplementary Fig. 4D–G) at 7 dpf, which may partially reflect the defective features resulting from the various mutations, and might be positively correlated with the tumour incidence and malignancy rates in zebrafish with these mutations.

Differentially expressed genes in the gliomas observed in zebrafish with combinations of mutations

To illustrate the underlying mechanisms of gliomagenesis in zebrafish with various combinations of mutations, global transcriptome analyses of randomly selected brain tissues with glioma formation dissected from 3-month-old *nf1* KO, *nf1*;*tp53* cKO, *rb1*;*tp53* cKO fish, and the brain tissues from *gfap*^{WT} controls, were performed (each sample contained three brains tissues harbouring tumours of *nf1* KO, *nf1*;*tp53* cKO, or *rb1*;*tp53* cKO fish, or three brain tissues of *gfap*^{WT} control fish). A total of 78, 122, and 104 significantly altered gene expressions were identified in *nf1* KO, *nf1*;*tp53*, and *rb1*;*tp53* cKO fish, compared with *gfap*^{WT} control (absolute $\log_2$ fold change > 2, $P < 0.05$), respectively (Fig. 6A, Supplementary Fig. 5A and Supplementary Table 5). KEGG signalling pathway analyses were subsequently performed to explore the potential functions of these differentially expressed genes in gliomagenesis in *nf1* KO, *nf1*;*tp53* cKO, and *rb1*;*tp53* cKO fish. The differentially expressed genes DEGs were clustered according to their functions and rankings based on the false discovery rate (FDR). The top 20 DEGs were mainly linked to the RTK/Ras/PI3K, cell cycle, Tp53, and focal adhesion signalling pathways (red marks; Fig. 6B, Supplementary Fig. 5B and C). Further examinations confirmed the expression of most gliomagenesis-related genes were altered in the tumours generated in zebrafish with various mutations (Fig. 6C, D and Supplementary Fig. 5D–F). The cluster analyses demonstrated the most significant altered gene expression, including Akt1, Raf, Egfr, Pdgf and Pdgfr, in the tumours from the fish with these three mutations (Supplementary Fig. 5G), strongly implicated the important role of the RTK/Ras/PI3K pathway in gliomagenesis (Furnari *et al.*, 2007). Notably, *tp53* mutation resulted in the aberrant expression of many cell cycle regulation-relevant genes, such as *Ccnd1*, *Ckd4*, *Ccne2*, *Cdc45*, *Ccnd3*, and *Pcna*, in *rb1* KO or *nf1* KO fish (Fig. 6D, Supplementary Fig. 5G and Supplementary Table 6). We also noticed that the tumours generated in *nf1*;*tp53* cKO fish were associated with the upregulation of Snail1a (Fig. 6C–E), suggesting that the activation of cell migration-relevant genes play important roles in Tp53-involved glioma development. In addition, histological analyses revealed the expression of Snail1a and Cyclin D1, two key factors of focal adhesion and cell cycle pathways, were much higher in intratumoral hypercellular nests of *nf1*;*tp53* cKO fish than in *nf1* KO fish (Fig. 6E and F). Furthermore, all above DEGs were almost undetected in *rb1* KO or *tp53* KO fish, indicating the mutation of *rb1* or *tp53* alone is insufficient to initiate gliomagenesis in zebrafish (Supplementary Fig. 5F).

To verify the mechanisms of tumorigenesis in zebrafish with various mutations, gene ontology (GO) analyses followed by network visualization of the enriched GO terms using BiNGO showed the downregulated genes were linked to apoptosis and cell death (Fig. 6G), and the upregulated genes were mostly involved in the cell cycle, proliferation, adhesion, migration, regulation of metabolic processes, development, and angiogenesis (Fig. 6H). Therefore, a simple schematic illustration displayed the factors regulated by RTK/Ras/PI3K, Rb1, Tp53 pathways, and their downstream signalling in tumours generated in *nf1* KO, *nf1*;*tp53* cKO, and *rb1*;*tp53* cKO fish (Supplementary Fig. 6). Importantly, most of the regulated factors, including the amplification of Egfr, Pdgfr, Ras, and Raf, as well as the Rb1-regulated G_1/S cell cycle checkpoint, were associated with RTK-related cell cycle progression (Supplementary Fig. 6).

Comparison of the molecular and histological signatures of gliomas in zebrafish and humans

UHC using the top 1000 probe sets was performed to analyse the altered gene expression profiles in tumours derived from *nf1* KO, *nf1*;*tp53* cKO, and *rb1*;*tp53* cKO fish. Three distinct subgroups were identified by hierarchical clustering (HC) of the segregated tumours (HC1–3). GO analyses of the altered gene expression revealed that the most significantly altered gene expression in HC1–3 was associated with cell cycle regulation, neuronal differentiation, and extracellular matrix–receptor interactions and cell adhesion, in glioma patients (Cancer Genome Atlas Research, 2008). Our results showed the tumours generated from *nf1* KO fish were present in the HC1 and HC3 subgroups; the tumours from *rb1*;*tp53* cKO fish were linked to all three subgroups; and *nf1*;*tp53* cKO background tumours were classified in the HC2 and HC3 subgroups (Fig. 7A). A previous study identified several subgroups, which were defined by comparing prognosis, including proneural, proliferative, and mesenchymal (mesenchymal), to recognize the dominant features that characterize each subgroup in human glioma (Phillips *et al.*, 2006). GSEA was performed using the subgroups of human glioma (Phillips *et al.*, 2006), and our gene

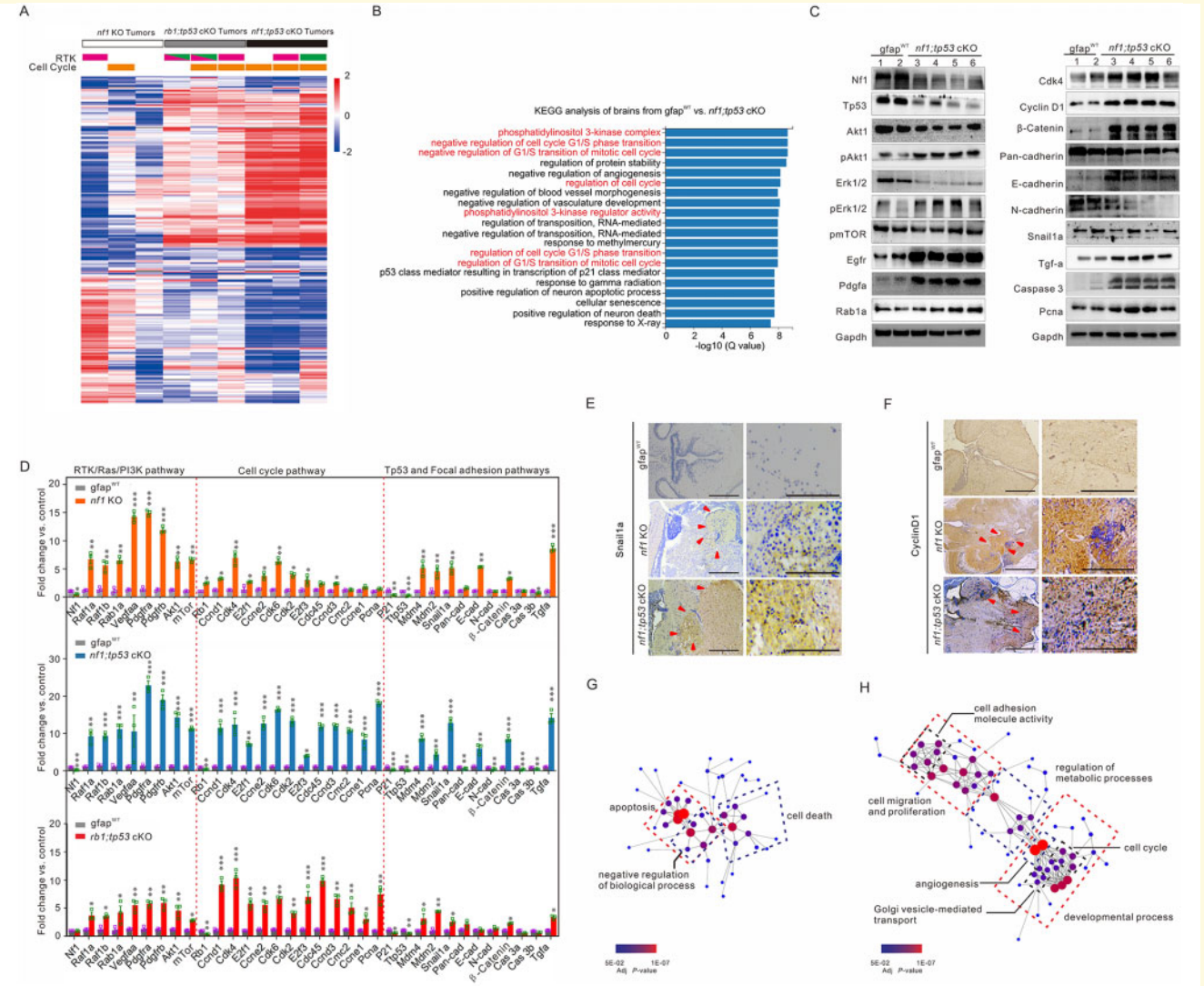

Figure 6 Identification of downstream signalling pathways in tumours generated in zebrafish with various mutations. (**A**) Heat map of differential expression genes based on the ratios identified the fold-changes indicating gains (red) and losses (blue) in the randomly selected brain tissues with glioma formation derived from 3-month-old *nf1* cKO (white bar), *rb1*;*tp53* cKO (grey bar), and *nf1*;*tp53* cKO (black bar) fish ($n = 3$ for each group). The amplifications of genes encoding RTKs Egfr (pink bars) and Pdgfra (green bars), as well as the amplification of cell cycle-related genes (Supplementary Table 6, orange bars) were also indicated. (**B**) KEGG pathway enrichment analyses of the tumours generated in *nf1*;*tp53* cKO fish. (**C**) Western blot determinations were performed to confirm the expression of the key gliomagenesis-related factors in *gfap*^{WT} (lanes 1–2) and *nf1*;*tp53* cKO tumours (lanes 3–6). (**D**) Relative expression of key factors of RTK/Ras/PI3K, cell cycle, and focal adhesion pathways in *nf1* KO, *rb1*;*tp53* cKO and *nf1*;*tp53* cKO fish, compared with *gfap*^{WT} control ($n = 3$ for each group). (**E** and **F**) Gliomas associated with *nf1* and *tp53* mutations showed stronger expression of Snail1a (**E**) and cyclin D1 (**F**), particularly in the hypercellular area (arrowheads). Scale bars = 100 μm. (**G** and **H**) Network visualization of GO terms associated with the downregulated (**G**) and upregulated genes (**H**) in brain tissues between *nf1*;*tp53* cKO and *gfap*^{WT} control.

set from the tumours derived from *nf1* KO, *nf1*;*tp53* cKO, and *rb1*;*tp53* cKO fish. As expected, genes recognized in the proneural, proliferative, and mesenchymal subgroups were significantly enriched in our gene sets, which were also altered among the expression signatures in our HC1–3 zebrafish subgroups (Fig. 7B–D and Supplementary Table 7). To verify the similarity between the gliomas generated from zebrafish and humans, we compared an additional four subgroups, including proneural, mesenchymal, neural, and classical subgroups, that associated with specific combinations of mutations, and identified by the Cancer Genome Atlas Project (Verhaak *et al.*, 2010). The results confirmed the significant similarity between the HC1 and proneural/neural subgroups, HC2 and proneural subgroups, HC3 and mesenchymal subgroups, respectively (Supplementary Table 7). Together, the gliomas generated from zebrafish were closely associated with the molecular signatures of human gliomas, especially a specific expression signature of the

mesenchymal subgroup, which mainly arose from the fourth ventricle in the zebrafish brain.

It is known that the proneural and neural subgroups are usually related to early-stage gliomas (grade I and II), and the mesenchymal subgroup is associated with high-grade gliomas (grade III and IV) (Phillips *et al.*, 2006). Our results showed that the tumours derived from *nf1* KO and *rb1*;*tp53* cKO fish mainly belonged to the proneural and neural subgroups, whereas the mesenchymal subgroup was mostly detected in the tumours generated from *nf1*;*tp53* cKO fish (Supplementary Table 7). Histologically, immunohistochemistry staining indicated significant similarity between the tumours derived from zebrafish and humans, as demonstrated by examining the expression of several key gliomagenesis-related genes, including *Gfap*, *Pcna*, pAkt, Snail, Nestin, and cyclin D1 (Fig. 7E–J). In this context, Cyclin D1 expression was associated with cell cycle regulation in HC1/proneural subgroups; Pcna plays important roles in HC2/proliferative subgroups; and Snail1a, pAkt, and Nestin were correlated with HC3/mesenchymal subgroups in either zebrafish or humans. Taking Pcna as an example, we found that the higher expression of Pcna in either humans or zebrafish was positively correlated with poor prognosis (Fig. 7K and L). In addition, similar tumour malignancy was found between humans and zebrafish with various mutations through analysing Pcna expression (Fig. 7M and Supplementary Table 8), suggesting that the underlying mechanisms of gliomagenesis in zebrafish and humans are probably identical, and these various zebrafish mutations may be helpful for precisely predicting the prognosis and malignancy in glioma patients with different mutational spectra.

Temozolomide treatment effectively suppresses gliomagenesis in zebrafish

To verify whether the treatment with TMZ, a DNA methylation agent with activity as a monotherapy for glioma treatment (Chinot *et al.*, 2004; Mirimanoff *et al.*, 2006), can inhibit gliomagenesis in zebrafish, we treated 14 dpf *nf1* KO and *nf1*;*tp53* cKO larvae with TMZ for up to 3 months. As expected, the results demonstrated that TMZ treatment significantly increased the survival rates of *nf1* KO and *nf1*;*tp53* cKO fish (Fig. 8A). Additionally, TMZ effectively suppressed gliomagenesis in *nf1* KO and *nf1*;*tp53* cKO fish (42.6% and 49.3%, respectively) (Fig. 8B).

Further histological analyses showed that TMZ treatment significantly reduced the expression of gliomagenesis-related key factors, including Pcna, pHH3, Gfap, Nestin, cyclin D1, and pAkt, in brain tissues from 3-month-old *nf1* KO and *nf1*;*tp53* cKO fish (Fig. 8C). In addition, quantification of the percentages of Pcna-positive cells showed significant reductions in the number of Pcna-positive proliferative cells in TMZ-treated 3-month-old *nf1* KO and *nf1*;*tp53* cKO fish (48.7% and 32.3%, respectively) (Fig. 8D). Taken together, the characteristics of TMZ-treated zebrafish with various mutations showed significantly lower mortality and cancer incident rates, as well as lower gliomagenesis-related immunoreactivities, which are partially similar to the histology of the patients with TMZ treatment (Nachbichler *et al.*, 2017; Rao *et al.*, 2017; Schreck and Grossman, 2018), suggesting that our models might constitute a valuable platform for both gliomagenesis studies and high-throughput screening of antiglioma compounds.

Discussion

Although mouse models have been widely used to understand the functions of tumour suppressors and oncogenes in tumorigenesis, tumour development, invasion and migration for decades, the zebrafish has become an increasingly popular animal model organism for cancer research in recent years (Feitsma and Cuppen, 2008; Bailey *et al.*, 2009; Peterson and Freeman, 2009). Specifically, the zebrafish model provides some unique advantages over the mouse model, including low-cost, high-fecundity, optical clarity, and the ability to perform high-throughput screening of drugs. Previous studies indicated that the mutations in tumour suppressors, such as *xmrk*, *tp53*, or *hag*, result in tumorigenesis of malignant peripheral nerve sheath tumours, melanoma, hepatocellular carcinoma, or neuroblastoma (Berghmans *et al.*, 2005; Amsterdam *et al.*, 2009; Dovey *et al.*, 2009; Li *et al.*, 2012*b*), whereas tumorigenesis can also be induced by the overexpression of oncogenes, such as *akt1*, *c-myc*, *kras*, or *braf*, in zebrafish (Langenau *et al.*, 2003, 2007; Patton *et al.*, 2005; Jung *et al.*, 2013). Recently, Yan *et al.* (2019) reported the generation of optically clear immunodeficient zebrafish, which can potentially be used for large-scale preclinical testing using the patient's own tumours.

Several groups have attempted to induce brain tumours in zebrafish. Amsterdam *et al.* (2009) reported that the zebrafish *hag* mutation can ultimately develop neuroblastoma-like tumours in cranial ganglia at 2 years of age through upregulating *fgf8* expression. A previous study showed that the overexpression of DAAkt1 alone resulted in a 36.6% glioma incidence in 6-month-old zebrafish (Jung *et al.*, 2013). However, because of longer incidence time and lower efficiency of gliomagenesis, these zebrafish models were not effective for studying gliomagenesis and drug screening. In mouse model, the combinations of mutations in *Pten*, *Tp53*, and *Rb1* can specifically induce high-grade astrocytoma (Holland *et al.*, 2000; Jacques *et al.*, 2010; Chow *et al.*, 2011), which encouraged us to efficiently develop glioma in zebrafish. Herein, the tissue-specifically expressed Cas9 expression driven by *gfap* promoter in gliocytes, the spinal cord, and retina in zebrafish (Bernardos and Raymond, 2006), allowed us to avoid the dysfunctions of these tumour suppressor in other tissues in zebrafish. Specifically, genes encoding tumour suppressors can be conditionally knocked out in gliocytes of brain tissues, and the positive

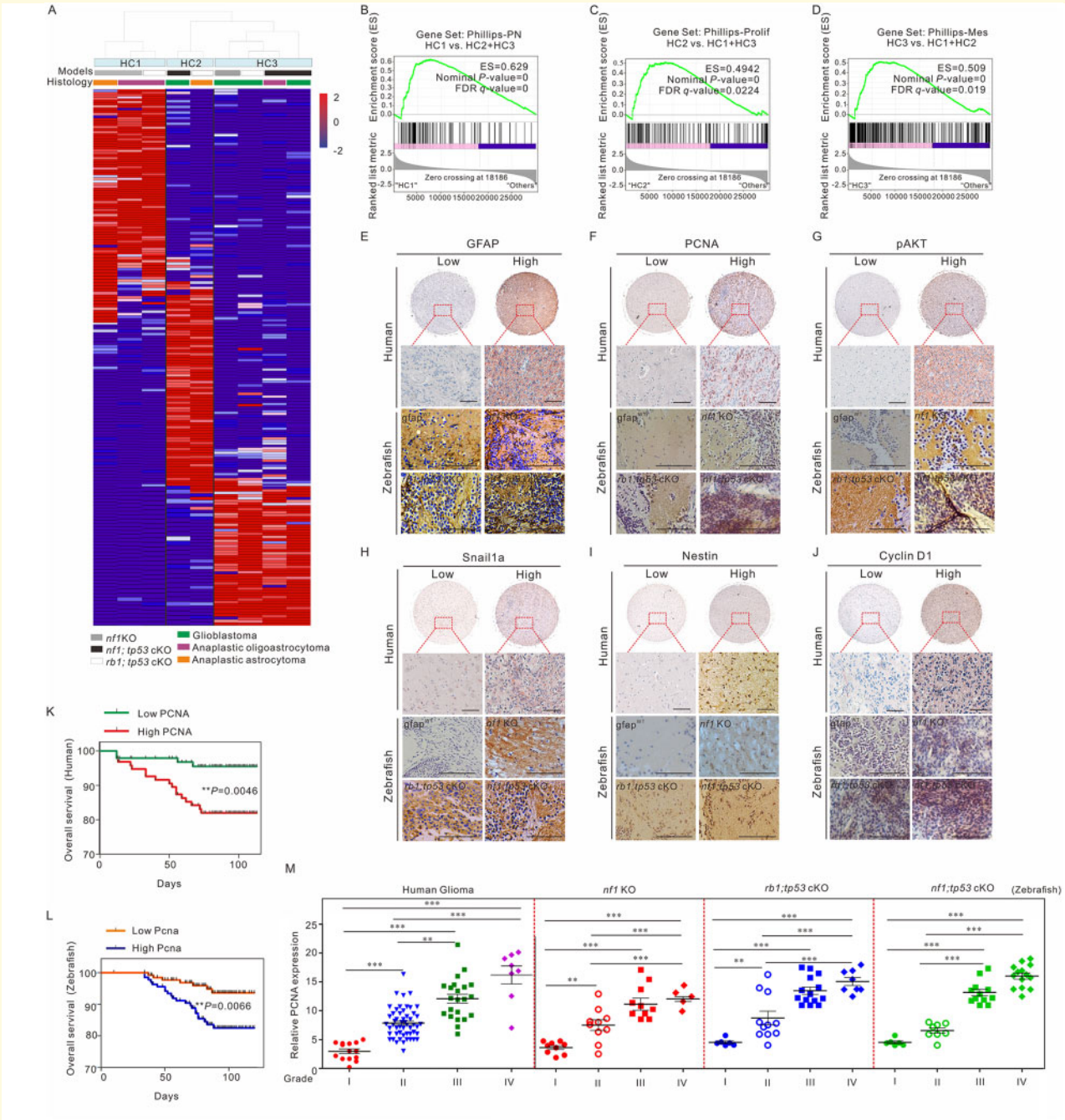

Figure 7 Molecular, histological, and prognostic comparison between zebrafish and human gliomas. (**A**) The global transcriptome of gliomas generated in *nf1* KO (grey bars), *nf1*;*tp53* cKO (black bars), and *rb1*;*tp53* cKO (white bars) fish were analysed by unsupervised hierarchical clustering (HC). The results showed the differential expression levels based on the median absolute deviation scores. Three primary clusters, HC1–3, and their dendrograms were shown at the *top* of the image. The heat map illustrated the most upregulated probe sets in each cluster derived using a linear model algorithm. The primary histological features were indicated with glioblastoma (green bars), anaplastic oligoastrocytoma (purple bars), and anaplastic astrocytoma (orange bars). (**B**–**D**) GSEA enrichment plots were drawn to compare each primary cluster with the other two clusters using three gene sets that define the expression subgroups of human gliomas, namely, Phillips-PN (proneural; **B**), Phillips-Prolif (proliferative; **C**), and Phillips-Mes (mesenchymal; **D**) subgroups. (**E**–**J**) Representative images obtained from the histological examination of the expression of several key gliomagenesis-relevant factors, including GFAP, PCNA, pAKT, Snail1a, Nestin, and Cyclin D1, in gliomas formed in human and zebrafish with different mutations ($gfap^{WT}$, *nf1* KO, *rb1*;*tp53* cKO, and *nf1*;*tp53* cKO fish). Scale bars = 100 μm. (**K** and **L**) Correlation between prognoses and Pcna expression in brain harboured tumours in humans ($n = 97$; **K**) and *nf1* KO fish ($n = 100$; **L**). (**M**) Correlation between glioma malignancy (grades I to IV) and PCNA expression in humans ($n = 97$), *nf1* KO ($n = 34$), *rb1*;*tp53* cKO ($n = 40$), and *nf1*;*tp53* cKO fish ($n = 39$). Data shown as mean ± SEM. $^{**}P < 0.01$, $^{***}P < 0.001$.

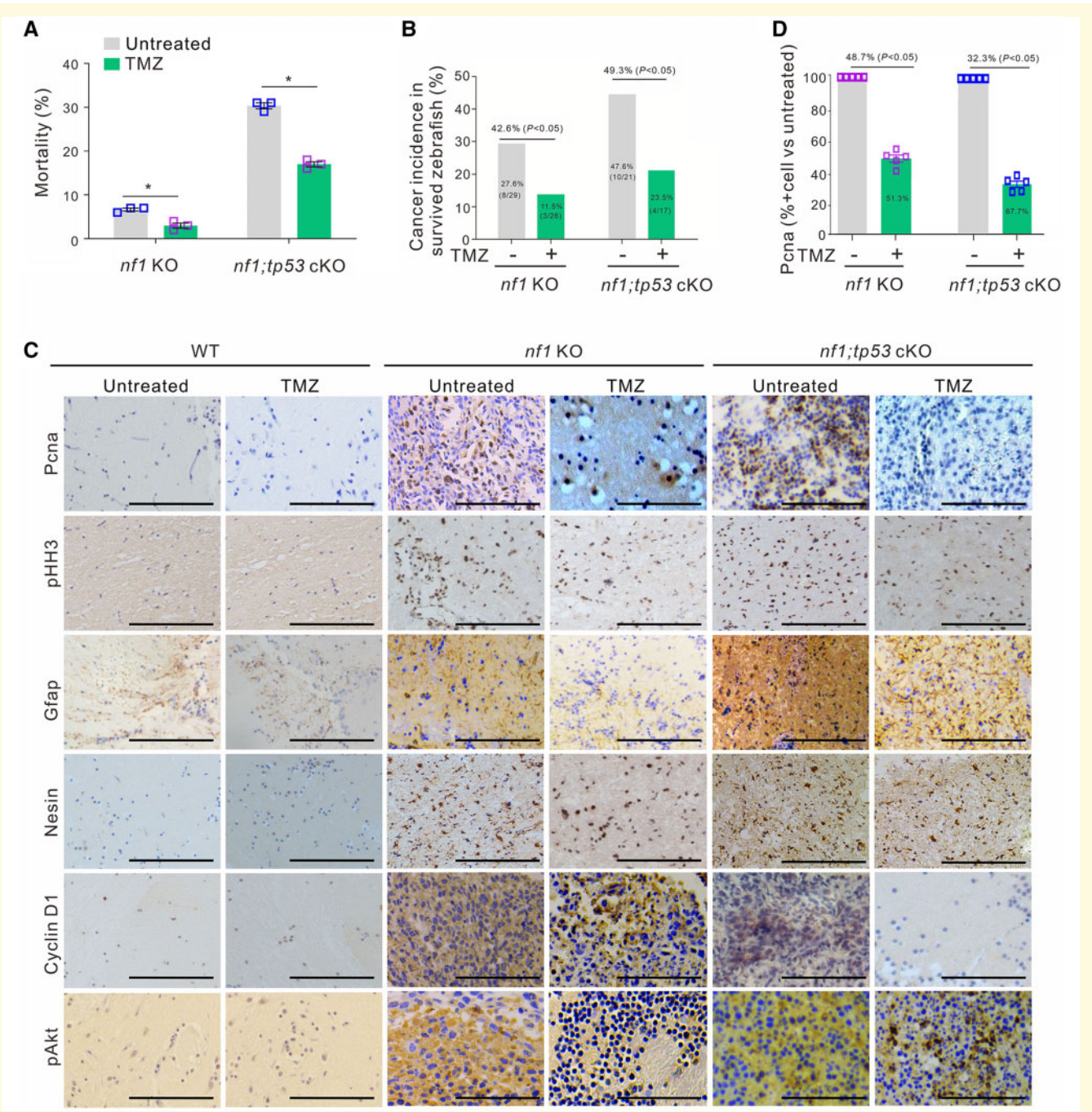

Figure 8 Temozolomide treatment inhibits gliomagenesis in *nf1* KO and *nf1*;*tp53* cKO fish until 3 months of age. (**A**) Mortality analyses of *nf1* KO and *nf1*;*tp53* cKO fish with or without TMZ treatment (n = 100 for each group; two groups for each line). (**B**) Tumour incidences were significantly suppressed by TMZ treatment in *nf1* KO and *nf1*;*tp53* cKO fish at 3 months of age (n = 100 for each group; two groups for each line). (**C**) Representative immunohistochemistry images examining the expression of Pcna, pHH3, Gfap, Nestin, Cyclin D1, and pAkt in *nf1* KO and *nf1*;*tp53* cKO fish with or without TMZ treatment. Scale bars = 100 μm. (**D**) Quantification of the percentages of Pcna-positive cells in *nf1* KO and *nf1*;*tp53* cKO fish with or without TMZ treatment (n = 5 random fields of view). Data shown as mean ± SEM. *$P < 0.05$.

tumorigenesis will be efficiently identified through *gfap* promoter-driving co-expression of *Cas9*, mCherry reporter, and specific gRNAs, such as *nf1*, *tp53*, or *rb1*, in zebrafish (Fig. 1A–C). Morphologically, an obvious 'bending-body' phenotype was initially observed at 2 months (Fig. 3C), and developed in a time-dependent manner in *nf1* KO, *nf1*;*tp53* cKO, *nf1*;*rb1* cKO, and *rb1*;*tp53* cKO fish lines (Fig. 5C). After the examinations of the post-mortem specimen in different parallel experimental groups, we confirmed that the 'bending-body' phenotype was induced by gliomagenesis-induced brain architecture disruption. In contrast, gliomagenesis was almost undetectable in the fish without bended

phenotype. Moreover, unlike triple cKO fish line (Supplementary Fig. 4A), there was undetected developmental disruption in spinal cord, regardless of bended phenotype, in all single and double mutants (Fig. 3B). We therefore expected that the gliomagenesis probably initiated in cerebellum (Fig. 2B), and the developed tumour gradually lead to the brain architecture disruption, which subsequently resulted in bended phenotype in zebrafish (Fig. 3C). Notably, the severely disrupted brain tissue probably jacked the cerebellum tectum to form 'visible bump' phenotype on the head of zebrafish (Fig. 4A). In addition, the percentages of gliomagenesis-related 'bending-body' phenotype were also directly associated with overall survival rates in different fish lines (Fig. 5B and C), suggesting that their principal lethal reason is probably due to the physical brain architecture disruption induced by glioma formation, and other gliomagenesis-related stress responses in zebrafish.

The mechanisms through which normal cells transform into malignant tumour cells are highly variable, and the specific genetic pathways, including the alteration of oncogenes and tumour-suppressor genes, contribute partially to tumorigenesis through certain arranged sequences (Zhu and Parada, 2002; Hanahan and Weinberg, 2011). As a key regulator of RTK/Ras/PI3K pathway, NF1 is involved in mediating various tumorigenesis-related biological responses, including cell proliferation, transcription, protein synthesis, and survival (Pal and Mandal, 2012; Wang *et al.*, 2017). *NF1* mutation has been detected in several malignant tumours, including malignant peripheral nerve sheath tumours and pheochromocytomas (Xu *et al.*, 1992; Legius *et al.*, 1993). Also, NF1 is known as one of most common inherited factors in cancer syndromes (Gutmann *et al.*, 1997). Previous report indicated most gliomas arising from *NF1* mutations can be characterized as belonging to mesenchymal subtypes (Verhaak *et al.*, 2010). *Nf1*-deficient mouse Schwann cells exhibit a growth advantage, and can readily be transformed (Kim *et al.*, 1997) to induce the initiation of neurofibroma formation (Zhu *et al.*, 2002). Our results revealed single *nf1* mutation induced a lower tumour incidence (Fig. 5D and E), and the activation of Akt1 (Fig. 3D), in zebrafish. Therefore, *nf1* mutation might be essential for the initiation of gliomagenesis (low-grade gliomas), and the subsequent glioma development might require additional genetic lesions.

RB1 is a key regulator of G_1/S checkpoint that regulates cell cycle progression to prevent uncontrolled proliferation. Mayhew *et al.* (2007) reported that RB1 deficiency significantly enhances diethylnitrosamine-induced hepatocarcinogenesis by increasing hepatocyte proliferation and compromising the integrity of the genome. The high mitotic activity, mainly induced by the frequently disrupted RB1/CDK/CKI regulatory cascade, is positively associated with the development of high-grade gliomas (grade III and IV) (Villanueva, 2011; Marshall *et al.*, 2019). In addition, ~80% of glioblastomas exhibit genetic alteration of RB1 pathway (Cancer Genome Atlas Research, 2008). In this study, the initiation of gliomagenesis was undetected in *rb1* KO fish during the first 6 months (Fig. 5E), suggesting that single *rb1* mutation might be insufficient for the initiation of gliomagenesis at early stage, but might be essential for the progression pathway. Notably, although not statistically significant, a trend towards higher percentages of high-grade gliomas was observed with the combination of *nf1* and *rb1* mutations at 3 and 6 months (Fig. 5D). Thus, the disruption of Rb1 pathway might contribute to the progression pathway of *nf1*-initiated gliomagenesis in zebrafish.

It is known that TP53 plays a major role in the maintenance of genome integrity by responding to various types of cellular stresses and inducing cell cycle arrest or apoptosis (Li *et al.*, 2012*a*; Muller and Vousden, 2013; Aubrey *et al.*, 2016). In glioma patients, *TP53* mutation have been observed at equal frequencies in all grades of gliomas (Rasheed *et al.*, 1994; van Meyel *et al.*, 1994). A previous study reported that the $tp53^{M214K}$ mutation alone can induce the development of malignant peripheral nerve sheath tumours in zebrafish with a tumour incidence of 5% after 12 months of age (Berghmans *et al.*, 2005), whereas the homozygous or heterozygous mutation of *Tp53* alleles in mice failed to induce gliomagenesis (Donehower *et al.*, 1992), which is consistent with the phenotype of *tp53* KO fish (Fig. 5E). Although TP53-deficient primary astrocytes exhibit increased growth and susceptibility to transformation (Bogler *et al.*, 1995), our results showed the mutation of *tp53* alone was still insufficient to initiate gliomagenesis at the first 6 months in zebrafish (Fig. 5E), and additional genetic or epigenetic events might be needed in this process. In addition, Vogel *et al.* (1999) showed that TP53 cooperates with NF1 to promote the development of malignant peripheral nerve sheath tumours in mice. The simultaneous disruptions of RB1 and TP53 pathways have been observed in 45% (9/20) of anaplastic oligodendrogliomas (Watanabe *et al.*, 2001). A recent study indicated that cooperativity among PTEN, TP53, and RB1 pathways can induce high-grade gliomas in adult brains in mice (Chow *et al.*, 2011). Thus, the phenotypes of *tp53*;*nf1* cKO fish can be potentially explained: *nf1* mutation initiates gliomagenesis, and *tp53* mutation subsequently promotes the progression pathway of glioma in zebrafish.

Integrative mutational and copy number analyses of the tumours derived from *nf1* KO, *nf1*;*tp53* cKO, and *rb1*;*tp53* cKO fish demonstrated gliomagenesis was mainly associated with three downstream pathways, including RTK/Ras/PI3K, cell cycle progression, and Tp53 and focal adhesion pathways (Fig. 6). RTK/Ras/PI3K pathway sustains proliferative signalling, contributes to the evasion of growth suppressors, the activation of cell invasion, the resistance of cell death. RTK usually undergoes receptor dimerization and autophosphorylation, recruit adaptor proteins, and activates downstream effectors, such as RAF/MEK/MAPK, PI3K/Akt, and Cdc42/Rac/Rho cascades. The results also showed the amplification of RTK activates its downstream effectors, including Akt1, Pdgf, Pdgfr, Egfr, and Raf, in *nf1* KO and *nf1*;*tp53* cKO fish (Fig. 6). The overexpression of PDGFR and its receptor in mouse brain revealed PDGF/PDGFR signalling

cascade is associated with gliomagenesis (Uhrbom *et al.*, 1998; Dai *et al.*, 2001). Additionally, as the most common target of *RTK* mutation (Furnari *et al.*, 2007), the alterations of *EGFR*, including amplifications, deletions, and single nucleotide polymorphisms (SNPs), have been identified in human gliomas, (Saadeh *et al.*, 2018). Besides, it is also known that Raf-mediated signalling cascade controls cell proliferation and differentiation. We thus hypothesized the alterations in these genes contribute to the initiation or development pathway of gliomagenesis in *nf1* KO and *nf1*;*tp53* cKO fish. Notably, the amplification of the effectors of the downstream of RTK pathway in *rb1*;*tp53* cKO fish (Fig. 6D), which is likely attributable to the combination of *tp53* and *rb1* mutations, might be essential for the initiation pathway of gliomagenesis in zebrafish.

It is noted that the initiation of gliomagenesis was only detected in *nf1* KO fish, but not in *rb1* KO or *tp53* KO fish even at 6 months (Fig. 5E), suggesting that the potential effects of *nf1* mutation is essential for gliomagenesis in zebrafish. The comparison of the molecular signatures between *nf1* mutant and the other two single mutants in fish brain tissue identified most of the key factors in RTK/Ras/PI3K pathway, including Raf1a, Raf1b, Rab1a, Vegfaa, Pdgfra, Pdgfrb, Akt1, and mTor, were significantly upregulated (>5-fold change, $P < 0.05$), in the brain tissue of *nf1* KO fish (Fig. 6D and Supplementary Fig. 5F), whereas only Vegfaa, Pdgfra, Pdgfrb, and Akt1 were slightly altered (average 2-fold change, $P < 0.05$) in the brain tissue in other two single mutants (Supplementary Fig. 5F), suggesting that the activation of RTK/Ras/PI3K pathway might be critical for gliomagenesis in zebrafish. Meanwhile, in cell cycle progression pathway, we found that Cdk4 and Cdk6 were extremely increased in *nf1* KO line (>5-fold change, $P < 0.05$) than in other two fish lines (less than 2-fold change, $P < 0.05$). It is known that CDK4/6 were not only fundamental drivers of the cell cycle and be required for the initiation and progression of various malignancies (Hamilton and Infante, 2016), but also associated with tumour immunogenicity in breast cancer (Goel *et al.*, 2017). Our finding indicated that the activation of Cdk4/6 was also essential for the initiation of gliomagenesis in zebrafish. In addition, the critical differences between *nf1* KO and other two single mutants were the upregulation of Snail1a, E-cadherin, and Tgfa (>5-fold change, $P < 0.05$), in Tp53 and focal adhesion pathways (Fig. 6D and Supplementary Fig. 5F), indicating that these three genes might play more important roles for the initiation of gliomagenesis.

KEGG and GO cluster analyses showed several cell-cycle regulators, such as Ccnd1, Cdk2, Cdk4, Cdk6, E2f1, and Pcna, were significantly regulated in *rb1*;*tp53* and *nf1*;*tp53* cKO fish (Fig. 6D), indicating cell cycle procession is mainly regulated by the Tp53 and Rb1 pathways. In response to the proliferative signals, RB is phosphorylated by CDK2, 4, and 6 (CDK2/4/6), and releases E2F transcription factors, which are associated with G_2/S transition and the initiation of DNA synthesis. In addition, CDK activity is positively regulated by cyclin D1 and E, and notably, aberrant CDK4 amplification has been identified in 14% glioma patients (Schmidt *et al.*, 1994). The aberrant CDK6, E2F1, cyclin D1, and cyclin E expression have also been detected in gliomas (Costello *et al.*, 1997; Buschges *et al.*, 1999; Chakravarti *et al.*, 2001). We therefore hypothesized that these regulators of cell cycle progression play important roles in the progression pathway of gliomagenesis in *nf1*;*tp53* cKO and *rb1*;*tp53* cKO fish. Furthermore, the cluster analysis revealed the aberrant focal adhesion pathway in tumours derived from *nf1*;*tp53* cKO fish, suggesting higher upregulation of Mdm2, Snail, β-catenin, and Tgfa expression might be responsible for the highest tumour incidence and malignancy rates found in *nf1*;*tp53* cKO fish (Fig. 5C–E).

GSEA analysis demonstrated the significant similarity in molecular signatures between the HC1–3 subgroups in the gliomas derived from zebrafish and the corresponding proneural, proliferative, and mesenchymal subgroups of human gliomas (Phillips *et al.*, 2006; Verhaak *et al.*, 2010). The gene expression signatures of gliomas generated from zebrafish with various combinations of mutations indicated that the identical selective pressures drive gliomagenesis and generate similar characteristic gliomas in humans and zebrafish. Furthermore, it is known that ∼90% of gliomas contain exhibit at least one disruption in RTK/Ras/PI3K, TP53, or RB pathway (Cancer Genome Atlas Research, 2008). Although the similarities between gliomas generated from various combinations of zebrafish mutations might provide further insights into some of the more common features of human disease, the slight differences in tumour histology, molecular features, and prognosis in gliomas generated through multiple altered pathways might be more valuable for investigating relevant subgroups of gliomagenesis, and for precision medicine, which involves the tailoring of cancer treatments to the specific tumour characteristics of each individual glioma patient.

The zebrafish model provides a unique opportunity for the high-throughput screening of anti-cancer candidate drugs. The accessibility of acquiring a toxicity profile in a physiological context is an additional benefit of using zebrafish as a model for drug screening. We evaluated the effects of TMZ on tumour incidence and the regulation of oncogenic effectors with various combinations of mutations in zebrafish. Although the transgenic fish were received TMZ treatment before onset of symptoms, which might not be identical to the clinical treatment for the patients with glioma, the histological and prognostic results obtained from different TMZ-treated transgenic fish lines still partially reflect the outcome of glioma treatment in human. Furthermore, the behaviours tests of zebrafish larvae with various combinations of mutations (Supplementary Fig. 4) revealed that these larvae might be suitable for easily detecting the rescuing morphological and behavioural phenotypes after the treatment of anti-cancer compound candidate at a 96- or 24-well-plate scale (Zon and Peterson, 2005), indicating these zebrafish models would be the valuable

tool for cost-effective and high-throughput pharmacological screening.

Acknowledgements

We thank Dr Jian Zou (Zhejiang University) for providing the pCS-TP vector. We thank Dr Weijiang Zhao (Jiangnan University) for the critical comments on the manuscript.

Funding

This work was financially supported by National Natural Science Foundation of China (81572494 and 81872070), Natural Science Foundation of Guangdong Province (2015A030313440), Li Ka Shing Foundation Grant for Joint Research Program between Shantou University and Technion-Israel Institute of Technology, the Projects of Chongqing Science and Technology Committee (cstc2019jcyj-zdxmX0035 and CSTCCXLJRC201714), and the Sanming Project of Medicine in Shenzhen (SZSM201911003).

Competing interests

The authors report no competing interests.

Supplementary material

Supplementary material is available at *Brain* online.

References

Ablain J, Durand EM, Yang S, Zhou Y, Zon LI. A CRISPR/Cas9 vector system for tissue-specific gene disruption in zebrafish. Dev Cell 2015; 32: 756–64.

Alcantara Llaguno S, Chen J, Kwon CH, Jackson EL, Li Y, Burns DK, et al. Malignant astrocytomas originate from neural stem/progenitor cells in a somatic tumor suppressor mouse model. Cancer Cell 2009; 15: 45–56.

Amsterdam A, Lai K, Komisarczuk AZ, Becker TS, Bronson RT, Hopkins N, et al. Zebrafish Hagoromo mutants up-regulate fgf8 postembryonically and develop neuroblastoma. Mol Cancer Res 2009; 7: 841–50.

Aubrey BJ, Strasser A, Kelly GL. Tumor-suppressor functions of the TP53 pathway. Cold Spring Harb Perspect Med 2016; 6: a026062.

Bai Q, Garver JA, Hukriede NA, Burton EA. Generation of a transgenic zebrafish model of Tauopathy using a novel promoter element derived from the zebrafish eno2 gene. Nucleic Acids Res 2007; 35: 6501–16.

Bailey JM, Creamer BA, Hollingsworth MA. What a fish can learn from a mouse: principles and strategies for modeling human cancer in mice. Zebrafish 2009; 6: 329–37.

Barash U, Spyrou A, Liu P, Vlodavsky E, Zhu C, Luo J, et al. Heparanase promotes glioma progression via enhancing CD24 expression. Int J Cancer 2019; 145: 1596–608.

Berghmans S, Murphey RD, Wienholds E, Neuberg D, Kutok JL, Fletcher CD, et al. tp53 mutant zebrafish develop malignant peripheral nerve sheath tumors. Proc Natl Acad Sci USA 2005; 102: 407–12.

Bernardos RL, Raymond PA. GFAP transgenic zebrafish. Gene Expr Patterns 2006; 6: 1007–13.

Bogler O, Huang HJ, Cavenee WK. Loss of wild-type p53 bestows a growth advantage on primary cortical astrocytes and facilitates their in vitro transformation. Cancer Res 1995; 55: 2746–51.

Brisbin S, Liu J, Boudreau J, Peng J, Evangelista M, Chin-Sang I. A role for C. elegans Eph RTK signaling in PTEN regulation. Dev Cell 2009; 17: 459–69.

Brustle O, McKay RDG. The neuroepithelial stem cell concept: implications for neuro-oncology. J Neuro-Oncol 1995; 24: 57–9.

Buschges R, Weber RG, Actor B, Lichter P, Collins VP, Reifenberger G. Amplification and expression of cyclin D genes (CCND1, CCND2 and CCND3) in human malignant gliomas. Brain Pathol 1999; 9: 435–42.

Cancer Genome Atlas Research. Comprehensive genomic characterization defines human glioblastoma genes and core pathways. Nature 2008; 455: 1061–8.

Chakravarti A, Delaney MA, Noll E, Black PM, Loeffler JS, Muzikansky A, et al. Prognostic and pathologic significance of quantitative protein expression profiling in human gliomas. Clin Cancer Res 2001; 7: 2387–95.

Chinot O-L, Barrie M, Frauger E, Dufour H, Figarella-Branger D, Palmari J, et al. Phase II study of temozolomide without radiotherapy in newly diagnosed glioblastoma multiforme in an elderly populations. Cancer 2004; 100: 2208–14.

Chow LM, Endersby R, Zhu X, Rankin S, Qu C, Zhang J, et al. Cooperativity within and among Pten, p53, and Rb pathways induces high-grade astrocytoma in adult brain. Cancer Cell 2011; 19: 305–16.

Comisso E, Scarola M, Rosso M, Piazza S, Marzinotto S, Ciani Y, et al. OCT4 controls mitotic stability and inactivates the RB tumor suppressor pathway to enhance ovarian cancer aggressiveness. Oncogene 2017; 36: 4253–66.

Costello JF, Plass C, Arap W, Chapman VM, Held WA, Berger MS, et al. Cyclin-dependent kinase 6 (CDK6) amplification in human gliomas identified using two-dimensional separation of genomic DNA. Cancer Res 1997; 57: 1250–4.

D'Angelo F, Ceccarelli M, Tala GL, Zhang J, Frattini V, et al. The molecular landscape of glioma in patients with Neurofibromatosis 1. Nat Med 2019; 25: 176–87.

Dai C, Celestino JC, Okada Y, Louis DN, Fuller GN, Holland EC. PDGF autocrine stimulation dedifferentiates cultured astrocytes and induces oligodendrogliomas and oligoastrocytomas from neural progenitors and astrocytes in vivo. Genes Dev 2001; 15: 1913–25.

Diamandis P, Aldape K. World Health Organization 2016 classification of central nervous system tumors. Neurol Clin 2018; 36: 439–47.

Donehower LA, Harvey M, Slagle BL, McArthur MJ, Montgomery CA Jr, Butel JS, et al. Mice deficient for p53 are developmentally normal but susceptible to spontaneous tumours. Nature 1992; 356: 215–21.

Dovey M, White RM, Zon LI. Oncogenic NRAS cooperates with p53 loss to generate melanoma in zebrafish. Zebrafish 2009; 6: 397–404.

Dyson NJ. RB1: a prototype tumor suppressor and an enigma. Genes Dev 2016; 30: 1492–502.

Ethan C, Emek D, Nikolaus S, Taylor BS, Chris S. Automated network analysis identifies core pathways in glioblastoma. PloS One 2010; 5: e8918.

Feitsma H, Cuppen E. Zebrafish as a cancer model. Mol Cancer Res 2008; 6: 685–94.

Ferguson KL, McClellan KA, Vanderluit JL, McIntosh WC, Schuurmans C, Polleux F, et al. A cell-autonomous requirement for the cell cycle regulatory protein, Rb, in neuronal migration. Embo J 2005; 24: 4381–91.

Ferguson KL, Vanderluit JL, Hebert JM, McIntosh WC, Tibbo E, MacLaurin JG, et al. Telencephalon-specific Rb knockouts reveal enhanced neurogenesis, survival and abnormal cortical development. Embo J 2002; 21: 3337–46.

Freije WA, Castro-Vargas FE, Fang Z, Horvath S, Cloughesy T, Liau LM, et al. Gene expression profiling of gliomas strongly predicts survival. Cancer Res 2004; 64: 6503–10.

Furnari FB, Fenton T, Bachoo RM, Mukasa A, Stommel JM, Stegh A, et al. Malignant astrocytic glioma: genetics, biology, and paths to treatment. Genes Dev 2007; 21: 2683–710.

Ge Y, Wu S, Zhang Z, Li X, Li F, Yan S, et al. Inhibition of p53 and/or AKT as a new therapeutic approach specifically targeting ALT cancers. Protein Cell 2019; 10: 808–24.

Geiger GA, Fu W, Kao GD. Temozolomide-mediated radiosensitization of human glioma cells in a zebrafish embryonic system. Cancer Res 2008; 68: 3396–404.

Gladson CL, Prayson RA, Liu WM. The pathobiology of glioma tumors. Annu Rev Pathol Mech Dis 2010; 5: 33–50.

Goel S, DeCristo MJ, Watt AC, BrinJones H, Sceneay J, Li BB, et al. CDK4/6 inhibition triggers anti-tumour immunity. Nature 2017; 548: 471–5.

Goussia AC, Papoudou-Bai A, Charchanti A, Kitsoulis P, Kanavaros P, Kalef-Ezra J, et al. Alterations of p53 and Rb pathways are associated with high proliferation in bladder urothelial carcinomas. Anticancer Res 2018; 38: 3985–8.

Gutmann DH, Aylsworth A, Carey JC, Korf B, Marks J, Pyeritz RE, et al. The diagnostic evaluation and multidisciplinary management of neurofibromatosis 1 and neurofibromatosis 2. Jama 1997; 278: 51–7.

Halbig KM, Lekven AC, Kunkel GR. Zebrafish U6 small nuclear RNA gene promoters contain a SPH element in an unusual location. Gene 2008; 421: 89–94.

Hamilton E, Infante JR. Targeting CDK4/6 in patients with cancer. Cancer Treat Rev 2016; 45: 129–38.

Hanahan D, Weinberg RA. Hallmarks of cancer: the next generation. Cell 2011; 144: 646–74.

Holland EC, Celestino J, Dai C, Schaefer L, Sawaya RE, Fuller GN. Combined activation of Ras and Akt in neural progenitors induces glioblastoma formation in mice. Nat Genet 2000; 25: 55–7.

Jacques TS, Swales A, Brzozowski MJ, Henriquez NV, Linehan JM, Mirzadeh Z, et al. Combinations of genetic mutations in the adult neural stem cell compartment determine brain tumour phenotypes. Embo J 2010; 29: 222–35.

Jao LE, Wente SR, Chen W. Efficient multiplex biallelic zebrafish genome editing using a CRISPR nuclease system. Proc Natl Acad Sci USA 2013; 110: 13904–9.

Jung IH, Leem GL, Jung DE, Kim MH, Kim EY, Kim SH, et al. Glioma is formed by active Akt1 alone and promoted by active Rac1 in transgenic zebrafish. Neuro Oncol 2013; 15: 290–304.

Kim HA, Ling B, Ratner N. Nf1-deficient mouse Schwann cells are angiogenic and invasive and can be induced to hyperproliferate: reversion of some phenotypes by an inhibitor of farnesyl protein transferase. Mol Cell Biol 1997; 17: 862–72.

Kim HJ, Lee HJ, Kim H, Cho SW, Kim JS. Targeted genome editing in human cells with zinc finger nucleases constructed via modular assembly. Genome Res 2009; 19: 1279–88.

Kwan KM, Fujimoto E, Grabher C, Mangum BD, Hardy ME, Campbell DS, et al. The Tol2kit: A multisite gateway-based construction kit forTol2 transposon transgenesis constructs. Dev Dyn 2007; 236: 3088–99.

Langenau DM, Keefe MD, Storer NY, Guyon JR, Kutok JL, Le X, et al. Effects of RAS on the genesis of embryonal rhabdomyosarcoma. Genes Dev 2007; 21: 1382–95.

Langenau DM, Traver D, Ferrando AA, Kutok JL, Aster JC, Kanki JP, et al. Myc-induced T cell leukemia in transgenic zebrafish. Science 2003; 299: 887–90.

Legius E, Marchuk DA, Collins FS, Glover TW. Somatic deletion of the neurofibromatosis type 1 gene in a neurofibrosarcoma supports a tumour suppressor gene hypothesis. Nat Genet 1993; 3: 122–6.

Li T, Kon N, Jiang L, Tan M, Ludwig T, Zhao Y, et al. Tumor suppression in the absence of p53-mediated cell-cycle arrest, apoptosis, and senescence. Cell 2012a; 149: 1269–83.

Li Z, Huang X, Zhan H, Zeng Z, Li C, Spitsbergen JM, et al. Inducible and repressable oncogene-addicted hepatocellular carcinoma in Tet-on xmrk transgenic zebrafish. J Hepatol 2012b; 56: 419–25.

Luo JJ, Bian WP, Liu Y, Huang HY, Yin Q, Yang XJ, et al. CRISPR/Cas9-based genome engineering of zebrafish using a seamless integration strategy. FASEB J 2018; 32: 5132–42.

MacPherson D, Sage J, Crowley D, Trumpp A, Bronson RT, Jacks T. Conditional mutation of Rb causes cell cycle defects without apoptosis in the central nervous system. Mol Cell Biol 2003; 23: 1044–53.

Manning BD, Cantley LC. AKT/PKB signaling: navigating downstream. Cell 2007; 129: 1261–74.

Marshall AE, Roes MV, Passos DT, DeWeerd MC, Chaikovsky AC, Sage J, et al. RB1 deletion in RB-pathway disrupted cells results in DNA damage and cancer progression. Mol Cell Biol 2019; 39: e00105.

Mayhew CN, Carter SL, Fox SR, Sexton CR, Reed CA, Srinivasan SV, et al. RB loss abrogates cell cycle control and genome integrity to promote liver tumorigenesis. Gastroenterology 2007; 133: 976–84.

Mirimanoff RO, Gorlia T, Mason W, Van den Bent MJ, Kortmann RD, Fisher B, et al. Radiotherapy and temozolomide for newly diagnosed glioblastoma: recursive partitioning analysis of the EORTC 26981/22981-NCIC CE3 phase III randomized trial. J Cell Oncol 2006; 24: 2563–9.

Muller PA, Vousden KH. p53 mutations in cancer. Nat Cell Biol 2013; 15: 2–8.

Nachbichler SB, Schupp G, Ballhausen H, Niyazi M, Belka C. Temozolomide during radiotherapy of glioblastoma multiforme: daily administration improves survival. Strahlenther Onkol 2017; 193: 890–6.

Ohgaki H, Kleihues P. The definition of primary and secondary glioblastoma. Clin Cancer Res 2013; 19: 764–72.

Ostrom QT, Gittleman H, Truitt G, Boscia A, Kruchko C, Barnholtz-Sloan JS. CBTRUS statistical report: primary brain and other central nervous system tumors diagnosed in the United States in 2011-2015. Neuro Oncol 2018; 20: iv1–iv86.

Padmanabhan A, Lee J-S, Ismat FA, Lu MM, Lawson ND, Kanki JP, et al. Cardiac and vascular functions of the zebrafish orthologues of the type I neurofibromatosis gene NFI. Proc Natl Acad Sci USA 2009; 106: 22305–10.

Pal I, Mandal M. PI3K and Akt as molecular targets for cancer therapy: current clinical outcomes. Acta Pharmacol Sin 2012; 33: 1441–58.

Paquet D, Bhat R, Sydow A, Mandelkow EM, Berg S, Hellberg S, et al. A zebrafish model of tauopathy allows in vivo imaging of neuronal cell death and drug evaluation. J Clin Invest 2009; 119: 1382–95.

Parsons DW, Jones S, Zhang X, Lin JC, Leary RJ, Angenendt P, et al. An integrated genomic analysis of human glioblastoma multiforme. Science 2008; 321: 1807–12.

Patton EE, Widlund HR, Kutok JL, Kopani KR, Amatruda JF, Murphey RD, et al. BRAF mutations are sufficient to promote nevi formation and cooperate with p53 in the genesis of melanoma. Curr Biol 2005; 15: 249–54.

Peterson SM, Freeman JL. Cancer cytogenetics in the zebrafish. Zebrafish 2009; 6: 355–60.

Phillips HS, Kharbanda S, Chen R, Forrest WF, Soriano RH, Wu TD, et al. Molecular subclasses of high-grade glioma predict prognosis, delineate a pattern of disease progression, and resemble stages in neurogenesis. Cancer Cell 2006; 9: 157–73.

Rao JU, Coman D, Walsh JJ, Ali MM, Huang Y, Hyder F. Temozolomide arrests glioma growth and normalizes intratumoral extracellular pH. Sci Rep 2017; 7: 7865.
Rasheed BK, McLendon RE, Herndon JE, Friedman HS, Friedman AH, Bigner DD, et al. Alterations of the TP53 gene in human gliomas. Cancer Res 1994; 54: 1324–30.
Saadeh FS, Mahfouz R, Assi HI. EGFR as a clinical marker in glioblastomas and other gliomas. Int J Biol Markers 2018; 33: 22–32.
Schmidt EE, Ichimura K, Reifenberger G, Collins VP. CDKN2 (p16/MTS1) gene deletion or CDK4 amplification occurs in the majority of glioblastomas. Cancer Res 1994; 54: 6321–4.
Schreck KC, Grossman SA. Role of temozolomide in the treatment of cancers involving the central nervous system. Oncology 2018; 32: 555–60, 569.
Schultz LE, Haltom JA, Almeida MP, Wierson WA, Solin SL, Weiss TJ, et al. Epigenetic regulators Rbbp4 and Hdac1 are overexpressed in a zebrafish model of RB1 embryonal brain tumor, and are required for neural progenitor survival and proliferation. Dis Models Mech 2018; 11: dmm034124.
Shin J, Padmanabhan A, de Groh ED, Lee JS, Haidar S, Dahlberg S, et al. Zebrafish neurofibromatosis type 1 genes have redundant functions in tumorigenesis and embryonic development. Dis Model Mech 2012; 5: 881–94.
Solin SL, Shive HR, Woolard KD, Essner JJ, McGrail M. Rapid tumor induction in zebrafish by TALEN-mediated somatic inactivation of the retinoblastoma1 tumor suppressor rb1. Sci Rep 2015; 5: 13745.
Subramanian A, Tamayo P, Mootha VK, Mukherjee S, Ebert BL, Gillette MA, et al. Gene set enrichment analysis: a knowledge-based approach for interpreting genome-wide expression profiles. Proc Natl Acad Sci USA 2005; 102: 15545–50.
Symons M, Segall JE. Rac and Rho driving tumor invasion: who's at the wheel? Genome Biol 2009; 10: 213.
Thangavel C, Boopathi E, Liu Y, Haber A, Ertel A, Bhardwaj A, et al. RB loss promotes prostate cancer metastasis. Cancer Res 2017; 77: 982–95.
Thisse C, Thisse B. High-resolution in situ hybridization to whole-mount zebrafish embryos. Nat Protoc 2008; 3: 59–69.
Thurnher MM. 2007 World Health Organization classification of tumours of the central nervous system. Cancer Imaging 2009; 9: S1–3.
Uhrbom L, Hesselager G, Nister M, Westermark B. Induction of brain tumors in mice using a recombinant platelet-derived growth factor B-chain retrovirus. Cancer Res 1998; 58: 5275–9.
van Meyel DJ, Ramsay DA, Casson AG, Keeney M, Chambers AF, Cairncross JG. p53 mutation, expression, and DNA ploidy in evolving gliomas: evidence for two pathways of progression. J Natl Cancer Inst 1994; 86: 1011–7.
Villa C, Miquel C, Mosses D, Bernier M, Stefano AL. The 2016 World Health Organization classification of tumours of the central nervous system. Presse Med 2018; 47: e187–200.
Verhaak RG, Hoadley KA, Purdom E, Wang V, Qi Y, Wilkerson MD, et al. Integrated genomic analysis identifies clinically relevant subtypes of glioblastoma characterized by abnormalities in PDGFRA, IDH1, EGFR, and NF1. Cancer Cell 2010; 17: 98–110.
Villanueva T. Tumorigenesis: RB, lost in progression. Nat Rev Cancer 2011; 11: 3.
Vogel KS, Klesse LJ, Velasco-Miguel S, Meyers K, Rushing EJ, Parada LF. Mouse tumor model for neurofibromatosis type 1. Science 1999; 286: 2176–9.
Vousden KH, Lu X. Live or let die: the cell's response to p53. Nat Rev Cancer 2002; 2: 594–604.
Wang Q, Chen X, Hay N. Akt as a target for cancer therapy: more is not always better (lessons from studies in mice). Br J Cancer 2017; 117: 159–63.
Wang Y, Yang J, Zheng H, Tomasek GJ, Zhang P, McKeever PE, et al. Expression of mutant p53 proteins implicates a lineage relationship between neural stem cells and malignant astrocytic glioma in a murine model. Cancer Cell 2009; 15: 514–26.
Watanabe T, Yokoo H, Yokoo M, Yonekawa Y, Kleihues P, Ohgaki H. Concurrent inactivation of RB1 and TP53 pathways in anaplastic oligodendrogliomas. J Neuropathol Exp Neurol 2001; 60: 1181–9.
Westerfield M. The zebrafish book: a guide for the laboratory use of zebrafish (Danio Rerio). Eugene: University of Oregon Press; 2007.
Xu W, Mulligan LM, Ponder MA, Liu L, Smith BA, Mathew CG, et al. Loss of NF1 alleles in phaeochromocytomas from patients with type I neurofibromatosis. Genes Chromosom Cancer 1992; 4: 337–42.
Yamazaki D, Kurisu S, Takenawa T. Involvement of Rac and Rho signaling in cancer cell motility in 3D substrates. Oncogene 2009; 28: 1570–83.
Yan C, Brunson DC, Tang Q, Do D, Iftimia NA, Moore JC, et al. Visualizing engrafted human cancer and therapy responses in immunodeficient Zebrafish. Cell 2019; 177: 1903–14.e14.
Ye QH, Zhu WW, Zhang JB, Qin Y, Lu M, Lin GL, et al. GOLM1 modulates EGFR/RTK cell-surface recycling to drive hepatocellular carcinoma metastasis. Cancer Cell 2016; 30: 444–58.
Zhu Y, Ghosh P, Charnay P, Burns DK, Parada LF. Neurofibromas in NF1: Schwann cell origin and role of tumor environment. Science 2002; 296: 920–2.
Zhu Y, Parada LF. The molecular and genetic basis of neurological tumours. Nat Rev Cancer 2002; 2: 616–26.
Zon LI, Peterson RT. In vivo drug discovery in the zebrafish. Nat Rev Drug Discov 2005; 4: 35–44.